Towards Rogue Wave Characterization in False Bay, South Africa

University of Cape Town, South Africa

Written by
Nicholas M. Salonen

Supervisor: Marcello Vichi (University of Cape Town)
Co-supervisor: Christo Rautenbach (South African Weather Service)

A dissertation submitted to the Faculty of Science, University of Cape Town,
in complete fulfillment of the requirements for the degree of
Master of Science in Ocean and Atmospheric Science

November 28, 2019

Abstract

Rogue waves are extreme oceanic waves which exceed twice the significant wave height of the wave record. In False Bay, South Africa, a shallow sea mount called rocky bank was suggested by Shipley (1964) to be the cause for increased wave energy along the eastern periphery of False Bay, where it is not uncommon for coastal users, particularly rock fishermen, to be washed off of the rocky coastline. The shallow bathymetry associated with rocky bank refracts the incoming open ocean swell and is thought to focus the wave energy toward sections of this coastline. This investigation aims to understand which offshore wave conditions could be conducive to rogue wave development along the eastern periphery of False Bay, South Africa. To do so, the phase-averaging spectral wave numerical model SWAN was used to investigate various wave conditions which are known to enter False Bay. The focusing effect which rocky bank supposedly has on the incoming wave energy was investigated by deepening and shallowing rocky bank's depth. This study showed that rocky bank does cause a varying degree of wave focusing which appears to be most dependent on the wave period, with higher wave periods leading to greater extents of refraction. According to this study, the average conditions which impact the south-western coastline of South Africa are conducive to wave focusing by rocky bank and despite the rarity of rogue wave events, coastal users are still affected by them. Calm seas have the ability to mislead users that make use of these dangerous rocky coasts, when the event of a rogue wave in small seas can still be sufficient to wash a person into the sea. A study by de Vos & Rautenbach (2019) suggested that users are at a higher risk, for a variety of coastal activities, during (seemingly) good conditions due to the increased human exposure. Since this study only simulated monochromatic wave conditions, one would expect the results to be significantly different if multiple swell systems were simulated concurrently, as this introduces the possibility of the dispersive focusing mechanism for swells that travel at different speeds and thus increasing the likelihood of a rogue wave. The knowledge acquired from this study is a great step towards understanding the wave climate of False Bay. This information can be used to implement possible warning systems which would hopefully be respected by the community and ultimately lessen the lives lost to extreme waves along False Bay's 'Death coast'.

Declaration

I declare that this dissertation is my own, unaided work. It is being submitted for the Degree of Master of Science at the University of Cape Town. It has not been submitted before for any degree or examination at any other University.

Nicholas Salonen

November 28, 2019

Acknowledgments

Academic
I would like to extend my gratitude firstly to the Oceanography Department of the University of Cape Town for providing me with the facilities and supervision without which this dissertation would not have been possible. To my supervisors Marcello Vichi and Christo Rautenbach. Thank you for the time you have given to me over the course of my studies. I would like to extend further thanks to Christo Rautenbach for being an excellent supervisor. I have learned a lot and hope to learn more from you in the future.

Funding
Funding for my MSc was also provided by the University of Cape Town through various research scholarships and academic awards, namely the Vice-Chancellors Research Scholarship and the SA Croll Scholarship. I would also like to thank the University of Porto for giving me the opportunity to spend 6 months studying at a fine institution through the International Credit Mobility program made possible by Erasmus Mundus.

Data
The data used in this project/research was kindly provided via Defence Research by The Institute for Maritime Technology, A Division of Armscor SOC (Pty) Ltd.

General
Lastly, to my family. You have encouraged me throughout my career at the University of Cape Town and I am extremely grateful for all of the support which you have given to me over the years.

Contents

1. Introduction

Tales of giant waves engulfing sea-going vessels have been a part of maritime legend for centuries (Lawton, 2001), but only since the wave records from the shipping and oil industries were released to oceanographers in the 1970's did their existence become that of major scientific concern (Pelinovsky & Kharif, 2003). These extreme, powerful and destructive waves are known amongst oceanographers and mariners as rogue or freak waves. Due to the mechanisms which lead to rogue wave development, they can appear and disappear very suddenly (Pelinovsky & Kharif, 2003; Chabchoub *et al.*, 2011; Dysthe *et al.*, 2008) and since rogue waves represent a great concentration of wave energy, they can cause severe damage to any vessel which gets caught in its path with many such events leading to the loss of human life (Shipley, 1964; Nikolkina & Didenkulova, 2012; Müller *et al.*, 2005; Bitner-Gregersen & Toffoli, 2012; Pelinovsky & Kharif, 2003; Akhmediev *et al.*, 2009; Dysthe *et al.*, 2008). The general definition for a rogue wave (H_f), that is which is used within the oceanographic community, is the rogue wave threshold criterion. With this definition, a rogue wave occurs when a wave exceeds twice the significant wave height (H_{m0}) of an observed sea state where $H_f > 2H_{m0}$ (Müller *et al.*, 2005; Nikolkina & Didenkulova, 2012; Bitner-Gregersen & Toffoli, 2012; Pelinovsky & Kharif, 2003; Chabchoub *et al.*, 2011).

Rogue waves can develop in seemingly calm seas in a basin of any depth with or without the influence of a current field (Pelinovsky & Kharif, 2003). In the reviews by Dysthe *et al.* (2008) and Pelinovsky & Kharif (2003), the known mechanisms of rogue wave formation have been described, namely:

- Spatial focusing (description in section 2.3.2.1)
- Dispersive focusing (description in section 2.3.2.2)
- Nonlinear focusing (description in section 2.3.2.3)

These mechanisms cause waves of varying frequencies and wavelengths to superimpose on one another, leading to the vast concentration of wave energy as well as the generation of an extreme wave. For this to occur, swell needs to be propagating through the ocean. The wave systems which influence the south-western coast of South Africa are generated mostly by the passing of eastward propagating mid-latitude cyclones from the Southern Ocean. Waves, at their origin, are unorganised and are characterized by a broad wave spectrum with a large range of wave directions and frequencies. Over time, frequency and directional dispersion cause the wave spectrum to narrow and the chaotic sea state develops into organised swell which is what is observed along the south-western coast of South Africa (Veitch *et al.*, 2019). This study will focus on a small coastal embayment called False Bay and will investigate a bathymetrical feature at the bay's mouth called rocky bank and it's effect on H_{sig} and wave energy distribution along the eastern periphery of the bay. The shallow sea mount was suggested by Shipley (1964) to spatially focus incoming wave energy towards the eastern flank of False Bay via wave refraction.

False Bay is situated at the south-east coast of Cape Town, found at the south-western coast of South Africa. It is enclosed to the West, North and East by the Cape Peninsula, the southern extent of Cape Town and Cape Hangklip respectively and is illustrated by figure 3.7 in section 3.4.2. The bay is open towards the south and due to its location, it is influenced by both the western boundary "Agulhas" current and the eastern boundary "Benguela" current, leading to great biodiversity found within the bay (Pfaff *et al.*, 2019). The coastal area of False Bay (from Cape Point to Cape Hangklip) attracts both domestic and overseas tourists who contribute an estimated R 900 million (US$ 63 million) per annum in direct expenditure with approximately 80% and 14% being generated by the Cape Peninsula and the Kogelberg coast respectively (Pfaff *et al.*, 2019). Since the bay is used by the public for numerous types of activities, it is of utmost importance that awareness is raised regarding the dangers that exist within the coastal

marine environment. Safety precautions, such as shark spotters, have been implemented to avoid/lessen the chances of any shark related incidents, with shark spotters being located at many of the busier beaches in False Bay (Muizenberg, Kogelbay, Kalk Bay, Fishhoek). Educational signs are also prominent at these beaches, which aim to inform the reader about the more commonly occurring surf-zone events which can lead to injuries or worse.

Shipley (1964) accounts for the death of rock fisherman on the eastern periphery of False Bay in his early theoretical study of rogue waves in False Bay, with the most recent incident occurring on the 15th of June 2019 where an angler was washed off the rocks leading to an unfortunate death (NSRI, 2019). These freak waves can catch the fisherman without warning, washing them off of the rocky coast with many having lost their lives to such events. This section of coastline (from the Steenbras river mouth to as far south as Cape Hangklip) was aptly given the nickname the "Death Coast" due to the high fatality rate amongst these fishermen (Shipley, 1964). Shipley (1964) attributed the high strike rate of rogue waves along this coastline to wave refraction theory due to the shallow sea-mount located at the mouth of False Bay. It is therefore imperative that awareness is raised amongst the inexperienced and the experienced coastal users regarding the risk of a rogue wave along the Kogelberg coastline.

Very few studies exist regarding the wave climatology of South Africa (Veitch *et al.*, 2019). This study will investigate the offshore wave climate surrounding the Cape Peninsula and will analyze the resultant coastal wave conditions within False Bay using Deltares numerical spectral wave modeling tool SWAN (Simulating WAves Nearshore) aiming to determine which open ocean conditions may be conducive to rogue wave development in False Bay, South Africa. Since Shipley (1964) suggested that it is rocky bank at the mouth of False Bay which is responsible for spatially focusing the predominantly south-westerly swell toward the eastern periphery of the bay, we expect longer period swells to be more conducive to rogue wave development since these waves will be refracted to a greater extent than shorter period waves and therefore increasing the extent of wave energy focusing. Secondly, we also expect to observe much greater exceedances of the threshold value with respect to the freak wave height criterion (where $H_f > 2H_{sig}$) used

to define a rogue wave. The objective of this study is to establish the wave transformation effect which rocky bank may have on offshore conditions by creating permutations of wave conditions within realistic ranges of the wave diagnostics. Any knowledge gained from this investigation will increase the understanding of the wave climate within False Bay. This will allow for the improvement of coastal warning systems and forecasts and will hopefully reduce the number of incidents and fatalities along the Death Coast.

2. Literature Review

2.1 False Bay Morphology and Bathymetry

False Bay is a shallow, coastal embayment situated on the south-east coast of Cape Town, South Africa. It has been described as a basin with a rectangular shape having approximate dimensions of 35 km by 30 km with depths of less than 100 m (Dufois & Rouault, 2012). The bay was separated into four distinct geographical zones by Atkins (1970). These zones categorize sectors of the bay with similar bathymetric characteristics. These are the gently sloping north sector, the east and west zones and the deeper central zone. More recently, Advisian (2018) used the Delft3D numerical modelling system by Deltares to generate a bathymetry chart for False Bay. Their figure illustrates the four geographic zones described by Atkins (1970) very clearly but unfortunately does not include the bathymetrical variation associated with the shallow sea-mount called rocky bank, which is one of the primary focuses of the present study.

The shallow bathymetrical feature, known as rocky bank, is located just outside of False Bay at -34.4255°S 18.595°E. This sea-mount is the main focus of the present study since it was suggested by Shipley (1964) to focus wave energy towards the eastern periphery of False Bay via wave refraction. Figure 2.1 (Shipley, 1964) illustrates how the shallow sea-mount was expected to refract incoming wave energy towards a specific region of the coast within False Bay by Shipley (1964).

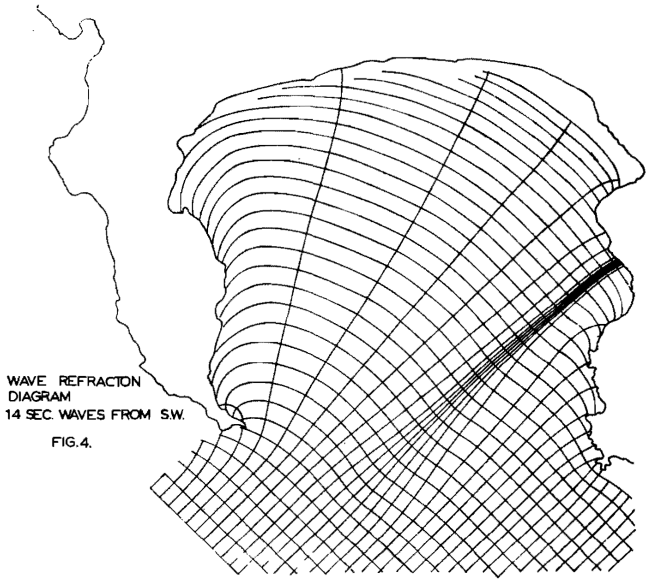

Figure 2.1: **This figure was taken from (Shipley, 1964).** A hand-drawn wave ray diagram with orthogonals for a 14 second period, south-westerly swell by Shipley (1964). This figure demonstrates wave refraction theory as the swell passes over rocky bank as suggested by Shipley (1964). The concentration of wave energy is indicated by the clustering of wave rays toward a small section of the eastern boundary of the bay. The same effect was observed for the same swell with 10 and 12 second periods (not shown).

2.2 Physical Characteristics of False Bay

2.2.1 Wave climate

The wave climate is the long-term sea state of an area. It is usually defined by analysing general trends in wave characteristics such as wave height (wave trough to crest), wave period (the time between waves which pass a fixed point) and wave direction (the direction from which they come from). Global patterns in wave climates have been linked with the atmospheric wind belts, with the largest waves occurring in temperate latitudes due to associated gale force westerly winds as well as strong frontal activity (Woodroffe, 2002). In the Southern hemisphere, the westerly wind belt is located between 30° - 60° S and the south-east trade winds occur between the equator and 30° S. The south-western coast of South Africa is located at approximately 34° S and is situated on the northern boundary of the westerly wind belt.

The synoptic weather conditions responsible for contributing toward the wave climate which the South African coastline experiences are described by MacHutchon (2006). These conditions are continental highs; west coast troughs; westerly atmospheric waves and cold fronts; cut-off lows and easterly atmospheric waves.

2.2.1.1 Wave Generating Mechanisms for the South African Coastline

The wind regimes associated with the different atmospheric weather patterns create sea waves which differ in characteristics such as direction, period and height due to variances in wind speed, wind direction and wind fetch (MacHutchon, 2006). Off both the east and west coasts of South Africa are semi-permanent sub-tropical high-pressure cells. The South Atlantic high-pressure cell is responsible for the short period waves ranging between 5 and 10 seconds which occur along the west coast and is also the system which produces the southerly swell which is observed primarily during austral summer (Theron *et al.*, 2013). The low-pressure systems, which are born in the westerly wind belt in the mid-latitudes, bring cold fronts from the south/south-west direction and are accountable for most wave conditions which affect the South African coastline (Theron *et al.*, 2013). Cut-off lows, which are not uncommon along the south-western coast of South Africa can also bring about extreme wave conditions especially during stationary periods (Theron *et al.*, 2013). These systems (cut-off lows and low pressure systems) can produce highly energetic long period swells (sometimes exceeding 20 seconds) which result in powerful local sea conditions (Theron *et al.*, 2013). Swells generated by frontal systems generally approach the west coast of South Africa from a westerly direction and the south coast from a south-westerly direction. During very intense storm events, significant wave heights (the average of the highest third of a wave record) have been recorded at over 10 meters (Theron *et al.*, 2013). Tropical cyclones do not feature along the south-western coast, but these systems do cause extreme conditions along the east coast which are comparable to those which are generated by cut-off lows (Theron *et al.*, 2013). This variety of wave generating mechanisms build up the wave climate which is observed around the south-western coastline of South Africa.

2.2.1.2 Wave Climate around South Africa

The wave climate of South Africa is known to vary seasonally in both wave intensity and direction (Theron *et al.*, 2013). This is caused by the northward shift of eastward propagating low-pressure systems in austral winter which is possible due to the comparable northward displacement of the South Atlantic high-pressure cell (Theron *et al.*, 2013). This results in an increase in wave height during austral winter months. Shipley (1964) and Theron *et al.* (2013) mention that the most common and persistent wave direction around the coast is from a south westerly origin, which is indicative of the passing low-pressure systems which produce the swell (Theron *et al.*, 2013). During austral winter, when the low-pressure systems travel east at a lower latitude (further north), the swell direction shifts to a more westerly direction along the Cape south-west coast (Theron *et al.*, 2013). The south-west coast experiences the largest waves with the wave height decreasing along both east and west coasts (Theron *et al.*, 2013).

2.2.1.3 Wave Climate of False Bay

False Bay is situated on the Cape south-west coast and experiences wave conditions which are generated by the variety of weather phenomena which occur over the South Atlantic Ocean. The swells which influence the bay are generated by the mechanisms discussed in section 2.2.1.1. Figure 3.4 on page 115 in (Theron *et al.*, 2014) illustrates the wave conditions as wave roses for a period from 1997-01-30 to 2008-12-01 for a station called 'Slangkop' (just off the west coast of the Cape Peninsula) with coordinates -34° S 17.5° E. These seasonal wave roses shown by their figure shows clearly the predominant swell direction to be south-westerly with a south-easterly component in summer and a west-north-westerly component in winter. However, False Bay is relatively sheltered from the predominant south-westerly swell which dominate the coastal waters. Theron *et al.* (2014) explains briefly and simply as to why the wave conditions within False Bay differ as much as they do using a figure generated by the numerical modelling tool SWAN.

Figure 2.2 on page 11 in Theron *et al.* (2014) is a standard output figure generated by the

model SWAN. Their figure displays H_{m0} using colored contours with wave direction vectors overlaid for the area of False Bay. Using this figure, Theron *et al.* (2014) accounts for the various processes which the swell undergoes as it propagates into False Bay. The external boundary conditions used to create their figure were a H_{m0} of 3 m, a T_p of 12 s and a south-south westerly wave direction of 202.5°. The wave height within the bay is noticeably smaller than the 3 m wave height along the external boundary. This reduction in wave height is a result of wave processes like refraction and friction. The most obvious reason for decreased wave heights in False Bay is attributed to the blocking of wave energy by the Cape Peninsula. Upon closer inspection of the southern most tip of the peninsula is almost a 2 m difference between wave heights observed inside and outside of the bay (Theron *et al.*, 2014). Their figure also shows the discrepancy in wave heights between the eastern (greater wave heights) and western periphery (smaller wave heights) of the bay. It is also along the eastern boundary of False Bay where Shipley (1964) showed evidence for wave focusing and the theorized development of rogue waves to occur.

2.3 Rogue Waves

2.3.1 Background Information

Rogue waves have been part of maritime folklore for centuries (Lawton, 2001; Dysthe *et al.*, 2008; Touboul *et al.*, 2006; O'Brien *et al.*, 2013). These extreme ocean waves are unexpectedly large, appearing suddenly on the sea surface (Pelinovsky & Kharif, 2003; Chabchoub *et al.*, 2011; Dysthe *et al.*, 2008; O'Brien *et al.*, 2013) and disappearing just as fast (Chabchoub *et al.*, 2011; O'Brien *et al.*, 2013). Terms such as "walls of water" and "holes in the sea" have been used to visually describe freak/rogue waves (Dysthe *et al.*, 2008). It was only in the 1970's when oceanographer's started collecting observations from the oil and shipping industries, leading them to believe in the existence of these monstrous waves (Pelinovsky & Kharif, 2003; Touboul *et al.*, 2006).

Observations from studies by Mori *et al.* (2002), Sand *et al.* (1990) and Hayer & Andersen (2000) suggest that rogue waves can form in a basin of any depth with our without the presence

of current fields (Touboul *et al.*, 2006). Not only due to the freakish size of rogue waves, but the characteristic whereby they emerge suddenly from the sea surface can result in a rogue wave causing severe damage to coastal and/or marine infrastructure and vessels. The crests of rogue waves can also be preceded and/or followed by deep troughs (holes) (Pelinovsky & Kharif, 2003; Osborne *et al.*, 2000), making these large waves even more dangerous to sea going vessels which are not anchored to the sea floor (Müller *et al.*, 2005). Incidents involving rogue waves are known to result in fatalities (Shipley, 1964; Nikolkina & Didenkulova, 2012; Müller *et al.*, 2005; Bitner-Gregersen & Toffoli, 2012; Pelinovsky & Kharif, 2003; Akhmediev *et al.*, 2009; Dysthe *et al.*, 2008) and large economic losses, making it an important area of oceanography to understand.

2.3.2 Rogue Wave Development Mechanisms

The review by Dysthe *et al.* (2008) lists the physical mechanisms which are suggested to be responsible for the development and formation of these giant waves. In the words of Dysthe *et al.* (2008), "Rogue waves represent a very high local concentration of wave energy compared with the average of the field, and a number of mechanisms are known to produce large waves from moderately small ones: spatial focusing, dispersive focusing, and nonlinear focusing."

2.3.2.1 Spatial focusing

Waves are naturally steered by the sea floor and will always propagate in such a way that the wave crests become aligned with the depth contour until the wave eventually steepens and breaks nearly parallel to the coastline in shallow coastal waters. Ocean waves begin to be influenced by the sea floor when the water column depth becomes less than half of the wavelength according to linear wave theory. Spatial focusing is the mechanism whereby variable bathymetry or variable current fields lead to the refraction of ocean waves. In areas where the coastline is irregular, wave energy hot-spots may exist which may be utilized as an energy resource through wave power devices as suggested by Halliday & Dorrell (2004).

Wave-current interactions have been greatly studied in the region of the Agulhas current (Mal-

lory, 1974; Shillington & Schumann, 1993; Grundlingh, 1994; Grundlingh & Rossouw, 1995). Scientists have observed extreme waves in the Agulhas current region during the passing of cold fronts with which strong winds and waves from the southwest are observed. Lavrenov (1998), showed that the current, which flows in a general south-westerly direction before it turns back on itself (known as retroflection), can trap waves within the boundaries of the current. This results in severe seas within the current band compared to the surrounding sea (Grundlingh, 1994). The sea surface elevation within the current was estimated by Grundlingh (1994) to be 100% greater, which agreed with TOPEX/Poseidon measurements (Grundlingh, 1994). When a group of unidirectional waves become trapped in a current, such as the Agulhas current, caustics (focusing points) can form near the refraction zones. Peregrine (1976) and Smith (1976) both suggested that amplification at these caustic zones can result in the development of extreme waves. However, a very small directional spread of the incoming waves causes the caustic zones to be stretched out, but this mechanism is still considered to be relevant for incoming waves which are close to being unidirectional (Dysthe *et al.*, 2008). In order to be able to study the formation of extreme waves at the caustics, numerical simulations and or analytical methods are required (Dysthe *et al.*, 2008).

2.3.2.2 Dispersive focusing

It is known that gravity waves are dispersive with phase and that the group velocities are inversely proportional with wave frequency (Dysthe *et al.*, 2008). A technique suggested by Longuet-Higgins (1974) demonstrates this effect and produces a short group of large waves at a given position in a wave tank. For this technique, a long wave group with linearly decreasing frequency (increasing period) is created. It is known that longer waves travel faster than shorter waves, and therefore the lower frequency waves at the end of the wave train will overtake the higher frequency waves (Touboul *et al.*, 2006). This wave train is known as a chirp. If it is correctly designed, the dispersive forces within the group force the wave group to contract to fewer wavelengths at a certain position (Dysthe *et al.*, 2008). The experimental results of a study by Touboul *et al.* (2006) illustrated the superposition of waves at a certain point and the subsequent defocussing of waves. Dispersive focusing is a linear effect and it can occur in linear

Gaussian seas during the rare occasion when the manufactured phase relations are such that a chirped wave train can develop (Dysthe *et al.*, 2008). Despite this wave train being simulated in wave tanks, the physical mechanisms able to create this sort of phase relation and chirped wave trains are not understood (Dysthe *et al.*, 2008). This mechanism of rogue wave formation showed slight differences in time-space evolution of the focusing wave train when Touboul *et al.* (2006) added the effect of wind to their experiment. Touboul *et al.* (2006) suggested that it was to be due to the wind generated surface currents. The similarly directed wind resulted in the focusing point to be shifted further downstream and a very slight increase in the amplitude of the wave was observed (see figure 5 in Touboul *et al.* (2006)). Not only did the experiment show a slight increase in wave amplitude, but the length of time for which the wave satisfied the rogue wave threshold was extended for increasing wind velocities. The numerical and experimental study by Touboul *et al.* (2006) yielded similar findings, however, due to the lack of any surface currents, the focusing point was not shifted further downstream.

2.3.2.3 Nonlinear focusing

According to the review by Dysthe *et al.* (2008), nonlinear focusing is the most studied topic with regard to the formation of rogue waves. This mechanism is studied theoretically, numerically and experimentally in wave tanks as it is theorized that this method may provide the necessary information when it comes to forecasting the occurrence of true rogue waves (Dysthe *et al.*, 2008; Fedele *et al.*, 2016). The basic physical mechanism is the 'Benjamin-Feir instability' and is suggested by many to be one of the nonlinear methods to understand rogue wave development (Pelinovsky & Kharif, 2003; Dysthe *et al.*, 2008; Chabchoub *et al.*, 2011). Since this study will focus on stationary monochromatic simulations, the nonlinear aspect is beyond the methodology of this study.

2.3.3 Defining a Rogue wave

During the investigations into the physics and mechanics behind rogue waves, several definitions for the occurrence of these unexpectedly high waves have been suggested (Pelinovsky & Kharif, 2003; Akhmediev *et al.*, 2009; Chabchoub *et al.*, 2011). The term "extreme wave" is said by

Pelinovsky & Kharif (2003) to "specify the tail of some typical statistical distribution of wave heights (generally a Rayleigh distribution)", whereas the term "freak wave" is used (again by Pelinovsky & Kharif (2003)) to "describe the large amplitude waves occurring more often than would be expected from the background probability distribution". The freak wave definition however, occasionally includes waves which are too high, too asymmetric and too steep (Pelinovsky & Kharif, 2003). The favoured definition is the freak wave amplitude criterion, where the wave height needs to be more than twice that of the significant wave height of a wave record (Müller *et al.*, 2005; Nikolkina & Didenkulova, 2012; Bitner-Gregersen & Toffoli, 2012; Pelinovsky & Kharif, 2003; Chabchoub *et al.*, 2011; Dysthe *et al.*, 2008; Onorato *et al.*, 2001). Pelinovsky & Kharif (2003) suggest that the use of statistical methods to make predictions based on data analysis is impractical and unproductive due to the rarity of rogue waves. However, the study by Touboul *et al.* (2006) showed, using a statistical approach, that the rogue wave phenomenon are not as uncommon as predicted by linear theories. Despite ongoing effort being put into understanding the nature of these hazardous waves, rogue wave records are insufficient and therefore the nature of these waves cannot be fully understood (Akhmediev *et al.*, 2009; Nikolkina & Didenkulova, 2012).

During the last 30 years, various approaches have been put forward aiming to understand the physics behind the appearance of rogue waves and its connection with oceanic and atmospheric factors (bathymetry, current field, wind and atmospheric pressure) (Pelinovsky & Kharif, 2003) as well as the probability of their occurrence (Dysthe *et al.*, 2008). In the review conducted by Dysthe *et al.* (2008), the foundation of rogue wave statistics is said to be well described by second-order random-wave theory. However, deviations from the model are not fully understood with Dysthe *et al.* (2008) suggesting that it could be the result of instrumental or sampling errors or that there are physical parameters missing from the model. Despite not always fitting this model, Dysthe *et al.* (2008) suggest that the second-order random-wave theory serves as a benchmark when comparing modelled and observed data.

2.3.4 Modelling a rogue wave

Over the years, various physical models have been developed and many laboratory experiments have been performed in order to provide information on the properties of rogue waves which is much needed for engineering purposes (Pelinovsky & Kharif, 2003). The consensus amongst oceanographers is that the existence of rogue waves cannot be explained by linear theories (Akhmediev *et al.*, 2009). The immense concentration of wave energy into a "wall of water" much greater than the significant wave height is thus left to be explained by nonlinear theories (Akhmediev *et al.*, 2009; Chabchoub *et al.*, 2011). One of these nonlinear theories is based on the nonlinear Shrödinger equation (Akhmediev *et al.*, 2009) and is the most direct method used to model the evolution of gravity water waves (Chabchoub *et al.*, 2011).

2.3.4.1 Nonlinear Schrödinger Equation (NLSE)

Osborne *et al.* (2000) investigated the rogue wave phenomenon from the perspective of the simplest known nonlinear wave equation which govern the deep-water wave trains. The fundamental nonlinear Schrödinger equations (Akhmediev *et al.*, 2009) were utilized for both 2- and 3-dimensional experiments. Osborne *et al.* (2000) set out to discover whether these equations and their higher-order extensions are able to predict rogue wave evolution, with the study showing that rogue waves are a generic property of deep water wave trains.

2.3.5 Rogue Waves in False Bay (Shipley, 1964)

The most in-depth (if not only) account of rogue waves in False Bay, South Africa, was conducted by Shipley (1964). His early account focused on wave refraction theory whereby ocean waves are redirected and "bent" when the depth of the water column changes. This theoretical study showed evidence that a shallow sea mount known as rocky bank at the mouth of False Bay is responsible for the focusing and concentrating of wave energy toward the eastern boundary of False Bay. The focusing of wave energy along this section of coast (nicknamed the "Death Coast" due to the frequent deaths of rock fisherman) lead Shipley (1964) to predict wave heights which exceeded the significant wave height by a considerable factor. Figure 2.1 shows the theorized

effect which rocky bank has on a 14 second period swell from the south-west. The focusing of wave energy toward the eastern flank is clearly illustrated in the figure. The refraction and subsequent focusing caused by rocky bank is considered to be responsible for the freak waves which occur within the bay, with such events having resulted in the loss of human life, with the most recent incident occurring on the 15th June 2019 (NSRI, 2019). Shipley (1964) concluded by contrasting calculated heights versus those which were physically observed. Following the "simple theory" which the study was based on, the calculated wave heights increased eastward from within the bay, with the greatest value being predicted to occur where most of the wave energy was focused. The observed and calculated wave heights corresponded well except at the location where the wave energy was supposedly focused by rocky bank. At this location, Shipley (1964) calculated a wave height of 1.8 m, but only observed a wave height of 0.6 m for a 1 m open ocean swell. Shipley (1964) attributed this difference to the wave losing energy, via bottom friction, as it passes over ever shallowing water. However, the observed wave heights along the eastern boundary were twice that of those along the more northern section of coast. Showing that this area is susceptible to more energetic conditions, with or without the occurrence of a rogue wave.

2.3.6 Application to the present study

The knowledge pertaining to the wave climate for the coast of South Africa is limited (Veitch *et al.*, 2019). This study will investigate the influence of rocky bank on wave conditions within False Bay, hoping to gain a better understanding of possible life-threatening extreme wave events which are known to occur (NSRI, 2019). The wave refraction theory used by Shipley (1964) will be taken into the numerical modelling realm where realistic wave conditions known to influence the bay will be simulated in SWAN to improve the knowledge of the general wave climate within False Bay and which conditions are most conducive to rogue wave formation.

3. Methodology

3.1 Introduction

Identifying the cause behind the increased wave energy and rogue wave occurrence along the eastern periphery of False Bay required the power of numerical modelling systems. For the present study, the phase-averaging spectral wave numerical modelling tool SWAN (Simulating WAves Nearshore) will be used to investigate wave conditions known to occur within the shallow bay. Early research conducted by Shipley (1964) showed us that rocky bank at the mouth of False Bay could be responsible for refracting, focusing and concentrating the predominantly south-westerly wave energy towards the eastern margin of False Bay. This process of wave energy focusing has led to many incidents along this stretch of coastline which have resulted in injury and even death (especially amongst rock fishermen). A methodology was therefore designed to develop an understanding as to which open ocean conditions are conducive to rogue wave development, as well as identifying the wave property (or properties) which is (are) most influential in leading to any extreme wave heights. To do so, an experimental structure was designed whereby permutations of wave conditions which are known to occur around the southwestern coast of South Africa were selected based on a 30-year hind-cast dataset produced by NCEP WAVEWATCH III model. For the present study, a range of H_{m0}, T_p and wave directions which influence False Bay were permuted to form the experimental foundation of the study. Furthermore, the profile of rocky bank was also manipulated to isolate its effect, as well as the value of the directional spreading associated with the modelled wave systems. This created 5 numerical experiments and are described in section 3.5.1. The simple tree diagram below illustrates simply how the various wave properties were combined with one another forming 990

permutations of possible wave conditions. In this chapter, the Delft3D-WAVE module SWAN, the data, the model set-up and the simulations will be described in detail.

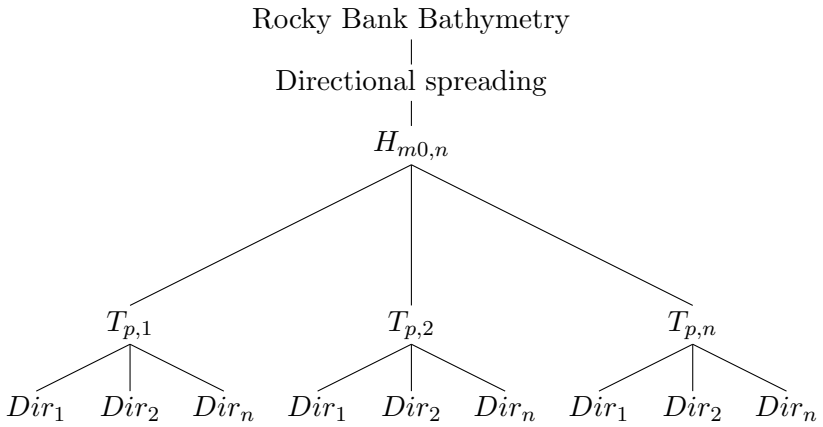

Figure 3.1: A simple schematic illustrating how the experimental design which is based on 990 permutations generated by combining all selected values of each wave diagnostic with the other. Changes to the directional spreading value and the rocky bank profile were held constant per simulation, creating 5 simulations in which the 990 recreated wave conditions were simulated.

3.2 SWAN

Investigating waves in coastal regions has been problematic for various wave modelling products (Booij *et al.*, 1999). To be able to model the complex interactions which occur within the coastal regions of our oceans, the open source software SWAN was designed specially to overcome these challenges (Booij *et al.*, 1999). This makes SWAN an ideal tool for the present study. The model itself was recently verified in a study by Williams (2019), who studied the effects on wave conditions within embayments surrounded by complex orographies, with False Bay being one of the study areas.

SWAN forms a part of a suite of modules which fall under the Delft3D modelling software and, more specifically, is the wave module of Delft3D, also known as Delft3D-WAVE. The wave software was developed in the Netherlands by the Delft University of Technology and was selected for this study due to its ability to resolve wave interactions in coastal regions. For the present study, version 4.01.00.hm of SWAN was used. SWAN, being a spectral wave model,

computes the change in wave energy as a function of wave frequency by solving the action balance equation (Booij *et al.*, 1999). Therefore, waves within the SWAN model are described by the two-dimensional wave action density spectrum (Booij *et al.*, 1999). The action density spectrum is equivalent to the energy density divided by the relative frequency $\left(N = \frac{E}{\sigma}\right)$ and is conserved in the presence of currents (Booij *et al.*, 1999). This spectrum, even in extremely nonlinear environments (i.e. the surf zone), can predict the spectral distribution of the second-order moment of the waves to a reasonable degree of accuracy (however, it may not be accurate enough to completely describe the waves statistically) (Booij *et al.*, 1999).

3.2.1 The Action Balance Equation

The spectral action balance equation - for Cartesian coordinates (i.e. x and y) - which describes the evolution of a wave spectrum, is shown below:

$$\frac{\partial N}{\partial t} + \frac{\partial C_x N}{\partial x} + \frac{\partial C_y N}{\partial y} + \frac{\partial C_\sigma N}{\partial \sigma} + \frac{\partial C_\theta N}{\partial \theta} = \frac{S_{tot}}{\sigma} \tag{3.1}$$

The first term on the left-hand side of equation 3.1 represents the local rate of action density with time, the next two terms represent propagation of action in geographical space x and y at velocities c_x and c_y respectively. The fourth term signifies the changes in relative frequency due to fluctuations in depth and currents. The final term on the left-hand side indicates depth and current-induced refraction. The expressions for the propagation velocity term "c" are taken from linear wave theory. The variable $S[= S(\sigma, \theta)]$ on the right hand side of equation 3.1 is the source term in terms of energy density. It characterizes the effects of generation and dissipation as well as the nonlinear wave-wave interactions. Descriptions of each term in the action balance equation are taken from (Booij *et al.*, 1999).

3.2.2 Wave energy source terms

S_{tot} can be expressed in two ways:

$$S_{tot} = S_{in} + S_{nl} + S_{ds'} \tag{3.2}$$

or,

$$S_{tot} = S_{in} + S_{nl4} + S_{ds,w} + S_{nl3} + S_{ds,br} + S_{ds,b} \tag{3.3}$$

On the right-hand side of equation 3.3, the first three terms represent deep water energy processes and the last three represent the shallow water energy processes. The different components of equation 3.3 are described by Gweba (2018): S_{in} represents the energy input from the wind, S_{nl} represents the non-linear wave-wave interactions and $S_{ds'}$ represents energy dissipation. For S_{nl} in deep water, quadruplet wave-wave interactions tend to dominate the development of the spectrum and transfer energy from the spectral peak to the higher and lower frequencies and the term is expressed as S_{nl4}. In the very shallow waters triad wave-wave interactions dominate and energy is transferred to higher frequencies and is represented as S_{nl3} (Booij *et al.*, 1999). The energy dissipation term $S_{ds'}$ consists of three elements: $S_{ds,w}(\sigma, \theta)$ to represent white-capping, $S_{ds,b}(\sigma, \theta)$ to capture the effect of bottom friction and $S_{ds,br}(\sigma, \theta)$ to include the impact of depth-induced breaking (Gweba, 2018)). Young (1999) advises that these factors are the major, but not the only factors, which effect the development of the wave spectrum.

3.2.2.1 Wind generation

The resonance mechanism of Phillips (1957) and the feedback mechanism of Miles (1957) is used in SWAN to describe the transfer of wind energy to the waves (Booij *et al.*, 1999). The source term which corresponds to these two mechanisms is represented by S_{in} and is typically

described as being the sum of both linear (A) and exponential (B) growth:

$$S_{in}(\sigma,\theta) = A + BE(\sigma,\theta) \tag{3.4}$$

Both A and B are dependent on the wind speed and direction as well as wave frequency and direction (Booij *et al.*, 1999). The apparent local wind speed and direction is used by SWAN to represent currents (Booij *et al.*, 1999).

3.2.2.2 Dissipation

The elements which make up the dissipation term of wave energy are white-capping, bottom friction and depth-induced breaking.

$$S_{in}(\sigma,\theta) = S_{ds,w}(\sigma,\theta) + S_{ds,b}(\sigma,\theta) + S_{ds,br}(\sigma,\theta) \tag{3.5}$$

Whitecapping, $S_{ds,w}$, results when a wave exceeds a certain steepness (Booij *et al.*, 1999) and is controlled by the pulse-based model of Hasselmann (1974). The source term $S_{ds,w}$ for this process is:

$$S_{ds,w} = -\Gamma_{kj}\tilde{\sigma}\frac{k}{\tilde{k}}E(\sigma,\theta) \tag{3.6}$$

$\tilde{k}$ and $\tilde{\sigma}$ represent the mean wave number and mean frequency respectively. Γ_kj is a coefficient which indicates the steepness of the wave and its value has been estimated by Komen *et al.* (1984).

The source term $S_{ds,b}$ represents the bottom-induced wave energy dissipation which can be due to bottom friction, bottom motion, percolation or backscattering on bottom irregularities (Booij *et al.*, 1999). For continental shelf seas with sandy bottoms, like False Bay, bottom friction seems to be the controlling mechanism and can be represented as:

$$S_{ds,b} = -C_{bottom}\frac{\sigma^2}{g^2\sinh^2(kd)}E\sigma,\theta \tag{3.7}$$

for which C_{bottom} is a bottom friction coefficient. SWAN accommodates three types of formulations for the bottom friction dissipation (Gweba, 2018). The present study will use the JONSWAP formulation.

Dissipation through depth-induced breaking occurs when waves steepen, become unstable and break as they enter shallower water. The expression of Battjes & Janssen (1978) can be used in SWAN to include this dissipation mechanism and is expressed as:

$$S_{ds,br}(\sigma,\theta) = \frac{D_{tot}}{E_{tot}} E(\sigma,\theta) \tag{3.8}$$

E_{tot} represents the total wave energy and D_{tot} is the total rate of energy dissipation caused by the breaking waves. D_{tot} is dependent on the water depth as well as the maximum wave height:

$$D_{tot} = -\frac{1}{4}\alpha_{BJ} Q_b \left(\frac{\tilde{\sigma}}{2\pi}\right) H_{max}^2 \tag{3.9}$$

In SWAN, $\alpha_{BJ} = 1$, $\tilde{\sigma}$ represents the mean frequency while Q_b defines the fraction of the wave breaking which is defined by the Rayleigh distribution:

$$\frac{1 - Q_b}{\ln Q_b} = -8\frac{E_{tot}}{H_{max}^2} \tag{3.10}$$

3.2.2.3 Nonlinear wave-wave interactions

SWAN models nonlinear interactions of wave energy using two types of wave-wave interactions. According to Booij *et al.* (1999), nonlinear wave-wave interactions occur as quadruplet or triad interactions. Quadruplet wave-wave interactions (S_{nl4}) dominate the development of the wave spectrum in deep water, while the triad wave-wave interactions, S_{nl3}, govern the shallow water. In SWAN, these interactions are expressed as:

$$S_{nl}(\sigma,\theta) = S_{nl3} + S_{nl4} \tag{3.11}$$

3.3 External Boundary Conditions

The wave climate which False Bay experiences is primarily controlled by the wave energy generated by the synoptic systems discussed by MacHutchon (2006) from the South Atlantic Ocean which surrounds the southwestern coastline of South Africa. It is important that the data which is used to identify the range of external boundary conditions are representative of this to account for the processes which the incoming wave energy will be influenced by.

A 30-year hind-cast dataset was used to identify the external boundary conditions for this study. This dataset was produced using a coarse resolution reanalysis product generated by NCEP (National Centers for Environmental Predictions) Climate Forecast System Reanalysis and Reforecast using the WAVEWATCH III (WW3) model (NWS, 2017). This data source was selected for this study as it is the same source of data used by the CSIR (Council for Scientific and Industrial Research) of South Africa. A reanalysis dataset is created via data assimilation during which actual observations are used to guide/correct the model's trajectory. For a reanalysis dataset, historical observations are used for the data assimilation.

The coarse resolution of the reanalysis dataset allows for the external boundary conditions for False Bay to be represented by one grid node and was extracted for the coordinates -34.5° S 18.5° E, a point approximately 15 km south of Cape Point. The 3-hourly time-series begins at 03h00 on the 01-01-1979 and ends at 00h00 on the 01-01-2010. The dataset consisted of the typical wave properties used to describe a wave climate. These being wave height, wave period and direction.

An accurate depiction of the bathymetry of False Bay is vital in order to capture the effects which features such as rocky bank and the steep bathymetry profiles of the east coast of False Bay have on the approaching wave energy. The data used to model the bathymetry was hydrographic data with the depth samples recorded at chart datum (lowest recorded sea levels). Within False Bay, the depth samples were of a very high resolution with approximately

4 samples per 0.5 km^2, while on the outside of the bay, the depth samples were expressed as transects/contours.

3.3.1 Wave Diagnostics

Ocean waves are made up of certain properties which dictate how fast they move, how they break and how much energy they transfer from the ocean to the coastline. The most relevant properties are described below and are the diagnostics which SWAN requires as input values when setting up the simulations.

1. **Significant Wave Height:** Various techniques are used to estimate significant wave height (H_{sig}). H_{sig} is considered as the average of the highest third of an observed wave field. If H_{sig} is calculated from a wave-by-wave analysis, it is denoted $H_{\frac{1}{3}}$. The significant wave height for this study is represented as H_{m0}. This indicates that the significant wave height is estimated from the variance of the observed wave field or as the integral of the variance of the spectrum (Engineers, 2002).

2. **Peak Period:** Symbolized as 'T_p', peak period represents the frequency of a wave system. Longer periods indicate longer wavelengths which indicates a greater concentration of wave energy.

3. **Peak Wave Direction:** Symbolized as 'θ_p', indicates the direction (in degrees) from where the wave energy comes from and coresponds with T_p.

These wave properties are the primary diagnostics used to describe a wave climate. From the 3-hourly 30-year hind-cast dataset, monthly climatologies (the average of each month over the duration of the timeseries) for H_{m0} and T_p were produced in Matlab$^{\text{TM}}$ (figure 3.2). The climatologies for the two wave diagnostics give a general understanding of the seasonality of the wave climate surrounding the Cape Peninsula. Figure 3.3 show seasonal wave roses for the mean wave directions which occur outside of False Bay with H_{m0} and T_p being added to the figures as the colour scales. Analysing figures 3.2 and 3.3 together provides a good understanding of the seasonal wave climate for the ocean surrounding the Cape Peninsula.

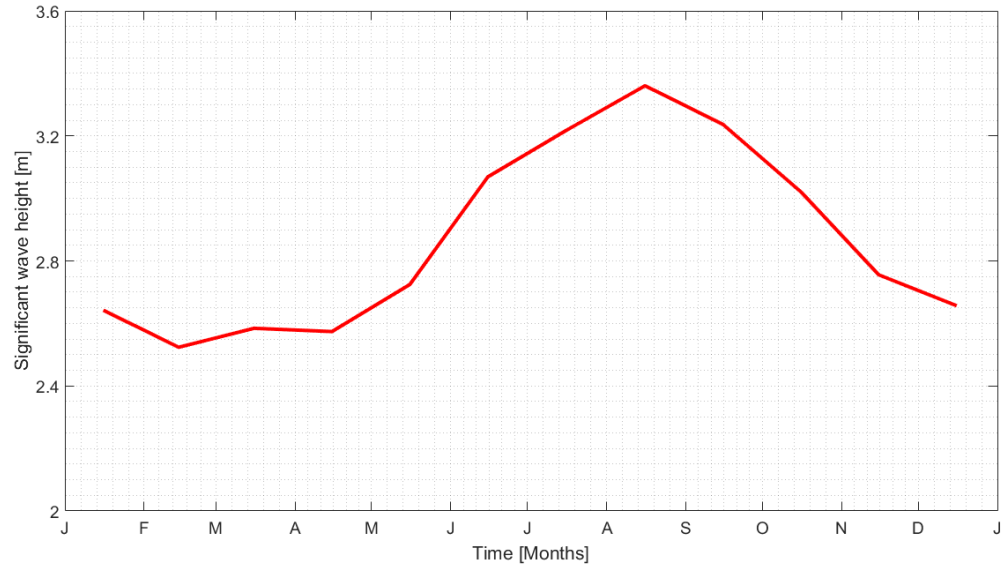

(a) H_{m0}

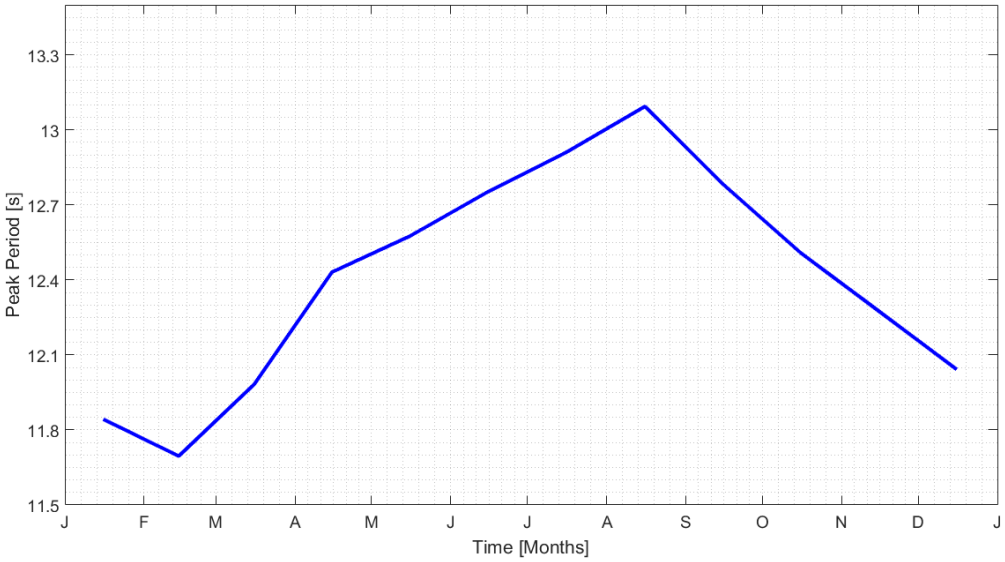

(b) T_p

Figure 3.2: Monthly climatology for significant wave height (figure 3.2a) and peak period (figure 3.2b) obtained from the NCEP reanalysis dataset produced by the WW3 model hind-cast. The figures show how both parameters increase during austral winter (April to October) which represents the northward shift in the synoptic weather patterns responsible for generating the waves that influence the southwestern coast of South Africa.

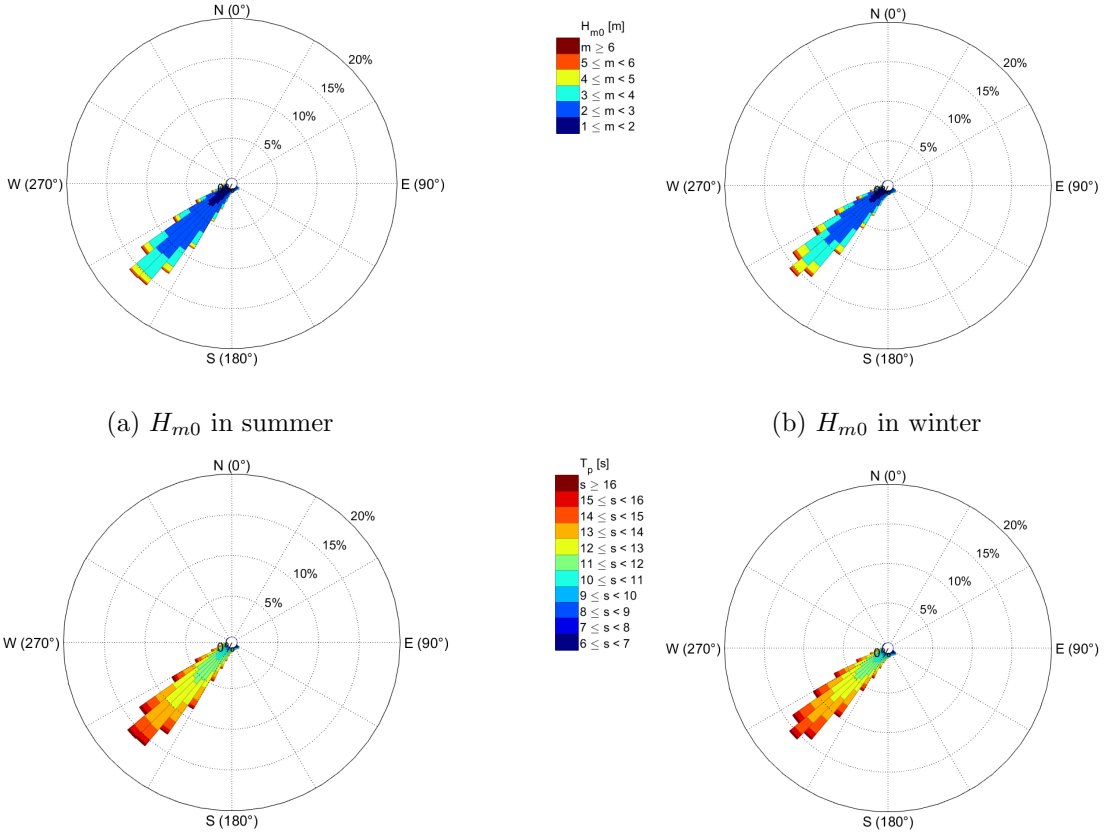

(a) H_{m0} in summer

(b) H_{m0} in winter

(c) T_p in summer

(d) T_p in winter

Figure 3.3: Seasonal wave roses showing the mean wave directions derived from the NCEP reanalysis dataset for outside of False Bay (-34.5° S 18.5° E). Wave roses 3.3a and 3.3b show the wave height proportions (as percentages) associated with 5° directional bins with wave roses 3.3c and 3.3d showing the same for peak period. The 30 year dataset describes the mean wave direction for the Cape south-west coast's wave climate to fall between 210° and 240°.

3.3.2 Wave Conditions

The wave conditions will be based on the wave diagnostics discussed in section 3.3.1 and will serve as the model forcings along the external boundaries of the study domain. Since the external boundary conditions will be incrementally increasing from low energy seas to extreme sea states, it is necessary to have an understanding regarding the ranges associated with each wave property and which wave conditions represent the average conditions around the southwestern coastline of South Africa. From figures 3.2 and 3.3, the overall impression of the wave climate which influences False Bay (according to the NCEP WW3 reanalysis dataset) can be described.

H_{m0} ranges, as a monthly average, from approximately 2.5 m in mid austral summer to roughly 3.4 m in mid-winter with the T_p ranging from approximately 11.7 s in mid-summer to 13.1 s in mid-winter. The wave roses (figure 3.3) show which wave directions occur the most at the mouth of False Bay and it is very clear that the southwesterly wave direction is the predominant direction with well over 50% of the wave energy approaching from between 210 - 240°. From these figures, the most frequently occurring wave conditions around the southwestern coastline of South Africa were identified, giving a clear impression of the seasonal wave climate.

It is important that the most frequently occurring conditions for each parameter are represented and characterized to determine which conditions can be classified as extreme. The co-occurrence plots (figure 3.4) show the co-occurrence of H_{m0}, T_p and wave direction. The figures show that the most commonly occurring conditions entering the mouth of False Bay are 1.6 – 3.7 m for H_{m0}, T_p between 10 – 14 s and wave directions between 200 – 250°. It is necessary to understand the subtleties which may derive from very small changes in the wave conditions. From these figures, the most typical and extreme sea states are identifiable, giving a range of wave conditions which may influence False Bay. These values were then chosen as the external boundary conditions for the numerical simulations computed using SWAN (see table 3.2 in section 3.5.1).

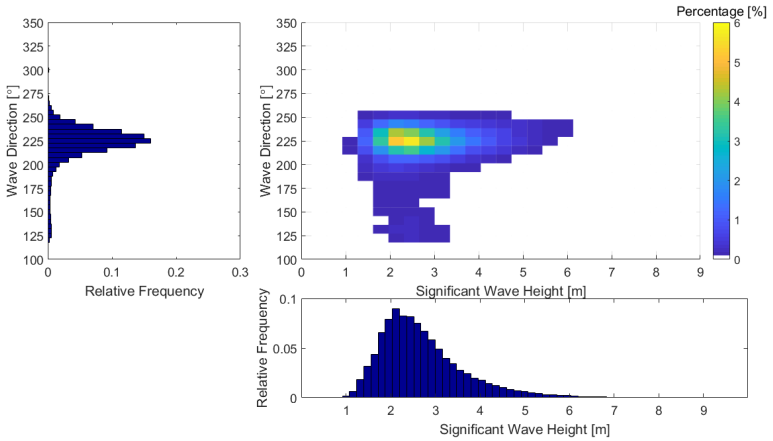

(a) H_{m0} and Direction

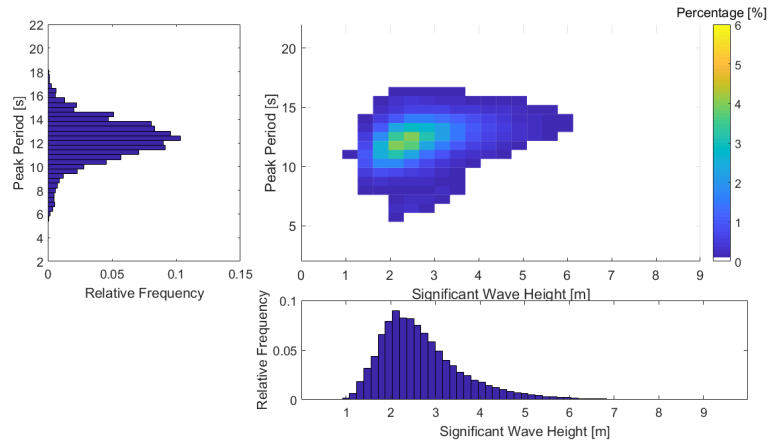

(b) H_{m0} and T_p

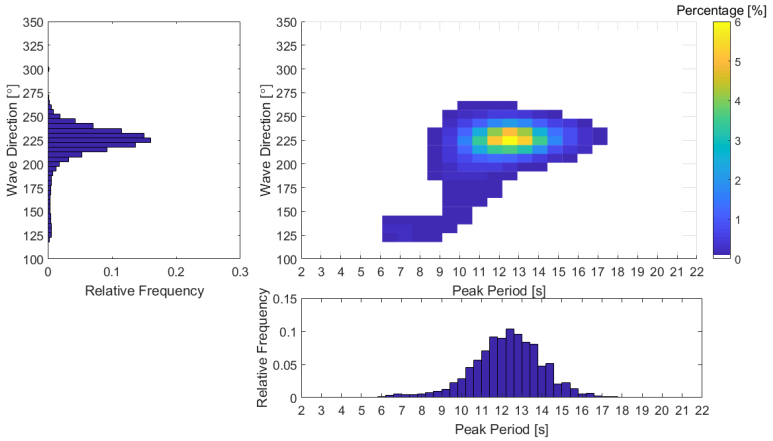

(c) T_p and Direction

Figure 3.4: Co-occurrence scatter plots showing the percentage of combined occurrence for significant wave height and mean wave direction (figure 3.4a), significant wave height and peak period (figure 3.4b) and mean wave direction and peak period (figure 3.4c). The colour scale indicates the percentage of observations for the co-occurring conditions with histograms for each variable showing their relative contributions.

3.3.3 Wave Spectra

Mathematical formulations have been developed to estimate wave spectra with various spectral models describing the range of frequencies that can occur during the randomness of the development of a sea state (Lakhan, 2003). The "JONSWAP" (Joint North Sea Wave Observation Project) spectrum has been used as the standard spectral model for wind-generated waves (Gweba, 2018) and was formulated during a a large scale project in the North Sea during 1968 and 1969 (Hasselmann *et al.*, 1973). The JONSWAP spectral model, also known as the modified Pierson-Moskowitz spectrum (Pierson & Moskowitz, 1964), has its foundation in the Phillips spectrum (Phillips, 1958).

3.3.3.1 JONSWAP Formulation

The Phillips spectrum (Phillips, 1958) characterizes the high frequency end of the wave spectrum (Violante-Carvalho *et al.*, 2002) and is written mathematically as:

$$S_P(\omega) = \frac{\alpha_P g^2}{(2\pi)^4}\omega^{-5} \tag{3.12}$$

This wave spectrum formulation of wind-generated ocean waves was based on the concept of an equilibrium frequency range assuming that the high frequency end of the spectrum is constrained by wave breaking with gravity being the controlling factor (Phillips, 1958).

The Pierson-Moskowitz spectrum (Pierson & Moskowitz, 1964) added a term to the Phillips spectrum which includes the lower frequency end of the expression. This new term in the equation describes a fully developed sea based on the thought that a fully developed sea state can be reached during consistent winds which blow over a large area. The expression which was added to the spectrum derived by Phillips (1958) is shown below:

$$S_{PM}(\omega) = \frac{\alpha_{PM} g^2}{(2\pi)^4}\omega^{-5} exp\left[-\frac{5}{4}\left(\frac{\omega_m}{\omega}\right)^4\right] \tag{3.13}$$

Since a fully developed sea state is extremely rare (Violante-Carvalho *et al.*, 2002), Hasselmann *et al.* (1973) investigated wind wave growth under fetch limited conditions.

The JONSWAP spectrum is a deep-water wind wave spectrum (Guo & Xu, 2011) and was formulated to represent the wave spectrum in a fetch limited environment (Gweba, 2018). The factor which the Pierson-Moskowitz spectrum is multiplied by describes the frequency spectrum for fetch limited waves, showing how waves continue to develop until they break on the coast. The full JONSWAP formulation is shown below:

$$S_J(\omega) = \frac{ag^2}{\omega^5} exp\left[-\frac{5}{4}\left(\frac{\omega_m}{\omega}\right)^4\right] \cdot \gamma^{exp\left(-\frac{(\omega-\omega_m)^2}{2\sigma^2\omega_m^2}\right)} \tag{3.14}$$

From Guo & Xu (2011): g is the gravitational acceleration, ω represents the wave frequency and α is the intensity of the spectrum concerning the wind speed (U which is taken at 10 m above sea level; eq. 3.15) and wind fetch length (x; eq. 3.16) and is calculated using the following equation:

$$\alpha = 0.076\bar{X}^{-0.22} \tag{3.15}$$

$$where, \bar{X} = \frac{gx}{U^2} \tag{3.16}$$

The peak wave frequency, ω_m, is the maximum frequency which occurs within the spectrum (Guo & Xu, 2011). This peak is defined mathematically as:

$$\omega_m = 22\left(\frac{g}{U}\right)(\bar{X})^{-0.33} \tag{3.17}$$

γ is the peak enhancement factor (PEF) and is used to represent the wind-wave growth state (Guo & Xu, 2011). Values for the PEF range between the values of 1.5 - 6 and have been suggested to be approximately 2.5 for South African waters (as suggested by the South African

Weather Service). The values for the peak shape factor σ are defined by:

$$\sigma = \begin{cases} 0.07, \omega \leqslant \omega_m \\ 0.09, \omega > \omega_m \end{cases}$$

The JOSNWAP spectrum, showing how the peak enhancement factor effects the broadness of the spectrum is shown below:

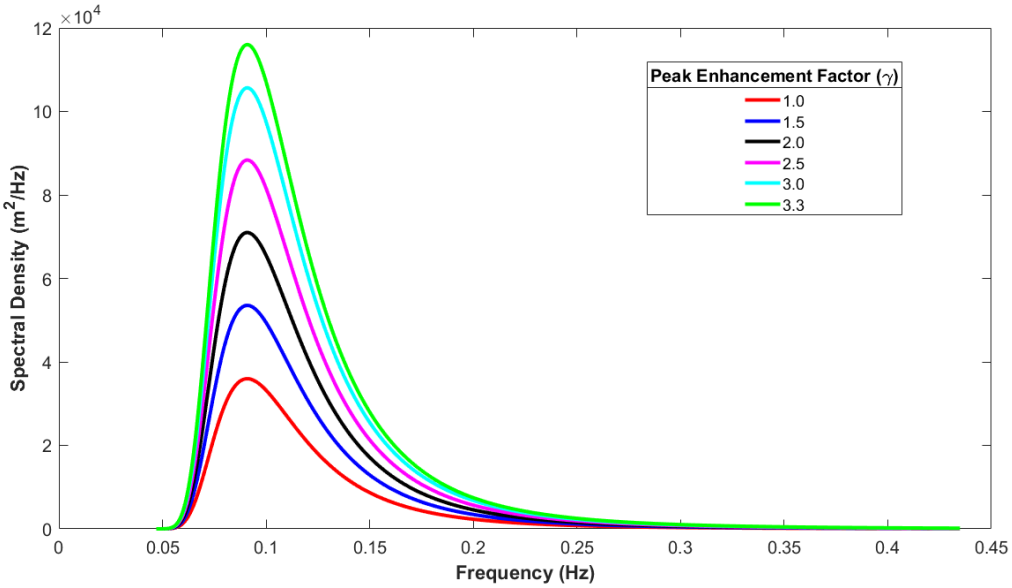

Figure 3.5: JONSWAP wave spectrum for varying PEF illustrating how the broadness of the spectrum gets narrower with increasing PEF (γ). Values for the spectrum parameters are 0.0081 for α (Gweba, 2018); 11 seconds for ω_m and between 1 and 3.3 for γ.

The values for the parameters α and γ of the JONSWAP spectrum for Cape Point were calculated from wave energy spectrum records spanning from 2014-06-01 till 2015-05-31 in Gweba (2018). Gweba (2018) estimated 0.001671 and 2.1417 for α and γ respectively. These values differed significantly from the default values set in SWAN which are 0.0081 for α and 3.3 for γ which are typical JONSWAP spectrum values for the North Sea (Guo & Xu, 2011).

3.4 Model Set-Up

3.4.1 Grid generation

The numerical model SWAN uses grids to define the study area. The external boundary conditions, defined by the wave diagnostics, propagate into the study domain from the grid boundaries (for more information on setting up the SWAN simulations, see Appendix A). The 30-year hindcast dataset, with these data being used to define the external boundary conditions, is located within the model boundaries at -34.5° S and 18.5° E.

The domain for the present study covers the entire area of False Bay and enough open ocean to account for the processes which the incoming waves will experience over the slowly shallowing water column. The left panel of figure 3.6 illustrates the extent of the study area. This will be referred to as the main grid which was set at a resolution of 500 m and, with its origin (lower left/south west corner) at approximately -34.8° 18.2°, extends 75 km east (approximately -34.5° 19°) and 87.5 km north (approximately -34° 18.2°).

Since the main area of interest for the current study is the eastern periphery of False Bay, grids with higher resolutions were positioned over this stretch of coast. Grid nesting, the process whereby higher resolution grids are overlaid within a main grid, is a process which will generate higher resolution output for the eastern flank of False Bay. At this location, two grids were nested within the main grid in order to establish a suitable grid resolution. Grid independence was then tested for to identify the suitable resolution (section 3.7). The resolutions of the nested grids were 150 m and 300 m. The right hand panel of 3.6 shows the 150 m resolution grid and the associated bathymetry contours (300 m grid not shown since the grid locations are identical).

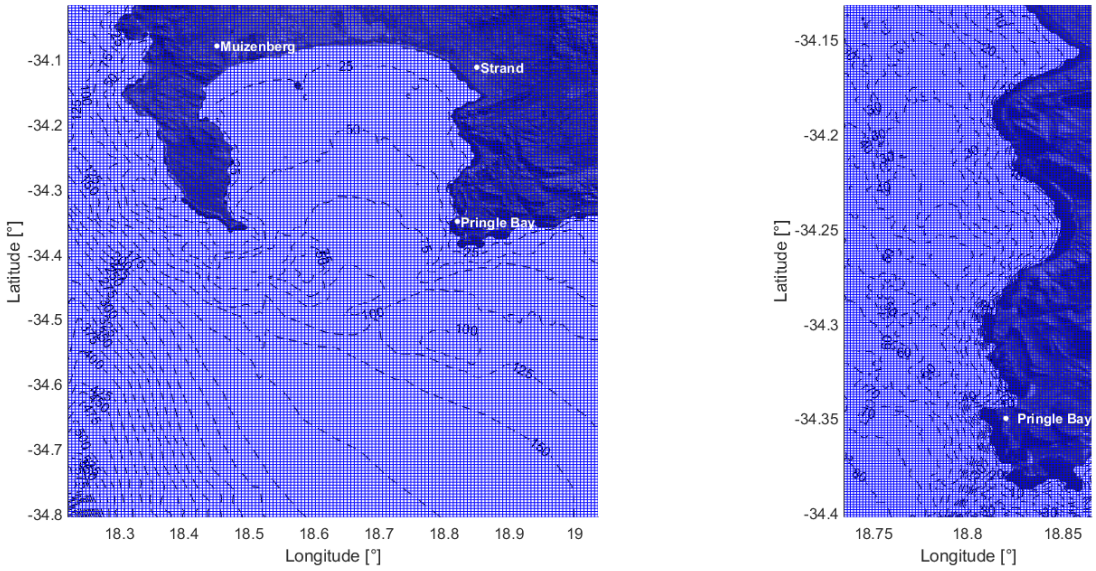

Figure 3.6: The left hand panel of the figure shows the main grid which covers the entire study area and defines the boundaries from which the wave conditions will propagate. The panel on the right illustrates the 150 m nested grid (300 m not shown) which is situated within the main grid along the eastern periphery of the bay. The small town called 'Pringle Bay' can be used as a place marker to visualise where the grid is situated.

3.4.2 Bathymetry

The depth samples for False Bay and the ocean surrounding the Cape Peninsula were imported into SWAN. The depth samples within False Bay were of a very high resolution with approximately 4 samples per grid cell (= 4 per 500 m^2). Outside of False Bay and to the west of the Cape Peninsula, the depth samples followed depth contours which extended outside of the study domain. From the depth samples a bathymetry profile can be generated in SWAN. To generate a bathymetry profile, the samples were interpolated in SWAN to define the grid nodes. The bathymetry for the control experiment is shown below.

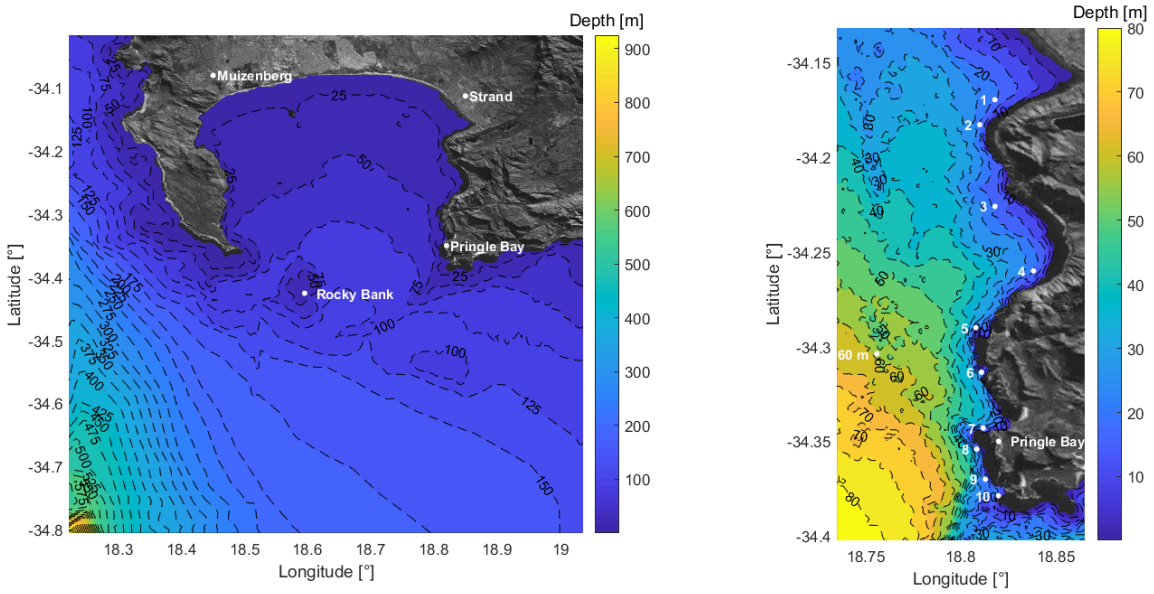

Figure 3.7: False Bay bathymetry generated by SWAN for the 500 m resolution main grid (left panel) and for the 150 m resolution nested grid (right panel). The location of rocky bank is shown in the main grid and is depicted using 25 m contours. The nested grid bathymetry is depicted using 5 m contour intervals and is shown on the right.

3.4.3 Diagnostic Points

To ensure that the correct wave conditions were propagating into the bay, a control point was located at -34.6700° 18.3187° with an associated depth of 400 m. This diagnostic point serves to verify the incoming wave conditions to ensure that the data is consistent with the external boundary conditions. Within False Bay, the diagnostic points all fall within the nested grid domain and aim to capture any differences in wave heights along this stretch of coast. At -34.3038° S 18.7558° E with a depth of 60 m, is a diagnostic point indicating the wave conditions which propagate into the nested domain (shown in figure 3.7). This point will be used for grid independence testing. Along the coast, 10 diagnostic points were placed along a 20 m depth contour. The northernmost point (near Strand) is diagnostic point 1 and the southernmost point (south of Pringle Bay) is diagnostic point 10. Table 3.1 shows the precise coordinates of each of these points which can be seen in 3.7:

Table 3.1: Diagnostic Point Locations along Eastern Periphery of False Bay

Diagnostic Point	**Latitude (°)**	**Longitude (°)**
1	-34.1697	18.8252
2	-34.1829	18.8159
3	-34.2278	18.8220
4	-34.2638	18.8383
5	-34.2925	18.8093
6	-34.3135	18.8109
7	-34.3441	18.8118
8	-34.3541	18.8085
9	-34.3700	18.8130
10	-34.3787	18.8198

3.5 Numerical Wave Simulations

The purpose of this investigation is to establish the open ocean wave conditions which are conducive towards rogue wave development in False Bay and also those which lead to an increase in wave energy at various locations along the eastern periphery of the bay. From figures 3.2, 3.3 and 3.4, it was possible to discern which open ocean conditions occur most often which then subsequently propagate into False Bay. These wave conditions were based on H_{m0}, wave direction and T_p. These conditions were then used as the external boundary conditions for the SWAN simulations. Once a range of of conditions were selected, different combinations of H_{m0}, wave direction and T_p were simulated to be able to see the effects which variations in the wave properties will have on the wave conditions within False Bay.

3.5.1 Model Forcing

Five wave simulations were completed for this study (S1 - 5). The external boundary conditions were established from the 30 year NCEP WW3 reanalysis dataset. From the dataset, a range of conditions for each wave property was identified. As illustrated by the tree diagram in section 3.1, permutations of known wave conditions around the southwestern coast of False Bay were combined in order to establish which wave property may be responsible for rogue wave

development along the eastern periphery of False Bay. Table 3.2 shows the range of values for each wave diagnostic and also describes the associated wave spectrum and bathymetry profiles for each simulation.

Table 3.2: Experimental structure for wave simulations performed in SWAN

Simulation	**Rocky Bank Profile**	**Directional Spreading** [°]	H_{m0} **[m]**	T_p **[s]**	**Wave Direction** [°]
S1 (control)	*Control*	24.9	1 - 9	6 - 20	180 - 270
S2	*Removed*	24.9	1 - 9	6 - 20	180 - 270
S3	*Raised*	24.9	1 - 9	6 - 20	180 - 270
S4	*Control*	22.9	1 - 9	6 - 20	180 - 270
S5	*Control*	27.6	1 - 9	6 - 20	180 - 270

3.5.2 Rocky Bank Variations

The identified conditions were manipulated such that each parameter was combined with each selected value of the other wave parameters. These permutations built the experimental foundation which should lead to a better understanding of rogue waves along the eastern periphery of False Bay. Not only were the wave parameters manipulated, but since Shipley (1964) suggested that the cause for increased wave heights and wave energy was due to wave refraction and spatial focusing by rocky bank, its depth and profile were also altered. The first experiment was designed as the control experiment (S1), where rocky bank was modelled to represent reality according to the depth samples. To see how much rocky bank impacts the distribution of wave energy in False Bay, it was removed entirely (S2). To do so, rocky bank was removed from a 70 m depth contour around the base of the sea-mount. This created a relatively flat sea floor with almost no variability. Rocky bank was also raised to identify the effect which a shallower and broadened sea-mount would have on the resultant wave conditions within the bay (S3). This was done by raising the 70 m depth base contour of rocky bank to a now broader and plateaued formation with a 24 m depth. To create a more realistic slope, the depth values from an 80 m depth were interpolated between the peak of the now raised rocky bank, which created a more

gradual rise.

3.5.3 Directional Spreading

The directional spreading property of a wave system indicates the spreading/narrowness of a wave system. A wave system with a low spreading factor will be more focused with less energy dissipation. A wave system with a broader spreading value will be less energetic as the energy is being spread/dissipated at a greater angle. For the present study, the control experiment (S1) used the typical directional spreading value for of 24.9° used to represent the ocean surrounding the Cape Peninsula. The narrower and broader spreading values were set at 22.9° and 27.6° and were the values used for simulations S4 and S5.

3.6 Model Verification

Verification of modelled data illustrates how well modelled data compares to observational data. Generally models do relatively well at producing reliable data, however, it is important to understand where the model may have biases. Knowing where a model may drift from reality is critical as it assists in understanding the behaviour of the model. To verify the output generated by SWAN, two locations within False Bay, where observational data was available (Miller's Point (MP) and Kogelbaai (KB), shown on figure 3.8), will be compared to the data generated by SWAN for the purposes of verifying the numerical simulations which were set for the present study.

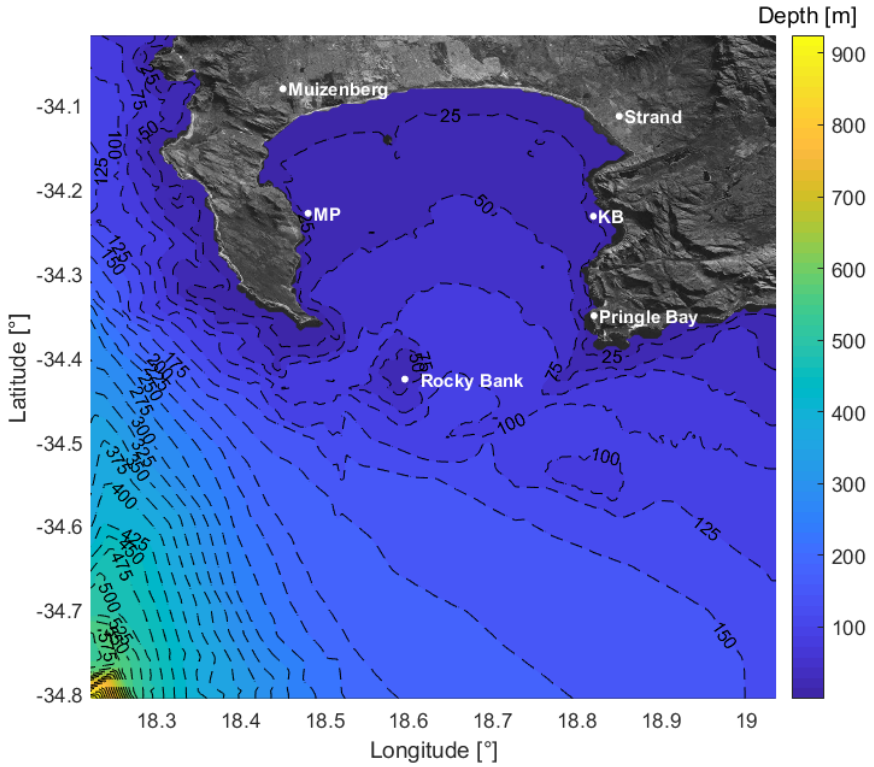

Figure 3.8: Model verification diagnostic point locations for Miller's Point (MP - western periphery) and Kogelbaai (KB - eastern periphery).

The first station, operated by the Council for Scientific and Industrial Research of South Africa (CSIR), is located within the area of apparent wave energy focusing within Kogelbaai. The wave data is measured using an ADCP (Acoustic Doppler Current Profiler) and is located precisely at -34.2317167° S 18.81916° E off the rocky cliffs of the Kogelbaai coastal reserve. The dataset is for the time period starting on the 20^{th} May 2015, ending on the 12^{th} August 2015. It is situated at a depth of approximately 23 m which is comparable to the depth of the diagnostic points used for the present study. The second observational dataset was provided by the Institute of Maritime Technology (IMT). The ADCP is located at Miller's Point at -34.228233° S 18.4847° E and is situated in a water column with a depth of approximately 25 m and is thus also comparable to the depth associated with the diagnostic points located along the eastern periphery of False Bay. The dataset provided by IMT begins in April 2014 and ends during March of 2019. From this dataset, a subset of continuous data was generated beginning on the

11^{th} February 2015 until the 1^{st} August 2015. To validate SWAN's output at MP and KB, 3-hourly NCEP WW3 operational data for H_{m0}, T_p and wave direction (NOAA, 2019) during June and July of 2015 were obtained for a location just outside of False Bay (at -34.5° S 18.5° E, the same extraction location as the 30-year hind-cast dataset) and served as the external boundary conditions for the model verification simulations.

Basic statistical measures were used to assess the overall performance of the model at KB and MP for H_{m0}. The verification process was based on the study by Williams (2019), who studied the importance of wind generated waves in embayments with complex orographic features with False Bay being used for one of the case studies. The statistical measures used to quantify the correctness of the modelled data are: the root mean square error - indicating the overall error of the modelled data (RMSE; eq. 3.18); the bias - indicates the model's tendency to over or under predict (eq. 3.19); the scatter index - indicates the ratio of the standard deviation to the mean of x (SI, eq. 3.20); and the Willmott index of agreement - indicates how well the modelled data compares to the observational data, where $0 \leq IA \leq 1$ with $IA = 1$ implying exactly equal values between observed and modelled data (IA; eq. 3.21) (Willmott, 1982). The equations below were used to calculate each index given a series of n model values y and the associated observational value x.

$$RMSE = \sqrt{\frac{\sum_{i=1}^{n}(y_i - x_i)^2}{n}} \tag{3.18}$$

$$bias = \sum_{i=1}^{n} \frac{1}{n}(y_i - x_i) \tag{3.19}$$

$$SI = \frac{\sqrt{\frac{1}{n}\sum_{i=1}^{n}(y_i - x_i)^2}}{\frac{1}{n}\sum_{i=1}^{n} x_i} \tag{3.20}$$

$$IA = 1 - \left[\frac{\sum_{i=1}^{n}(y_i - x_i)^2}{\sum_{i=1}^{n}(|\acute{y}_i| - |\acute{x}_i|)^2}\right];\ \text{where } \acute{y}_i = y_i - \bar{x}_i, \acute{x}_i = x_i - \bar{x}_i \tag{3.21}$$

3.7 Grid Independence

Grid nesting is a method where a smaller grid is located within another grid. This technique is used when an area of interest is located within a greater domain and a finer resolution is required to capture effects which occur at a smaller scale. For the current study, nested grids were located along the eastern periphery of False Bay, extending from the northern end of the eastern periphery near Strand extending past the southern extent of Cape Hankglip. Since this is the area of interest for the current study, it is important that the wave dynamics which occur in shallowing coastal waters are modelled as accurately as possible. To find an appropriate resolution, the nested grids were given resolutions of 300 m and 150 m and are within the 500 m main grid which encompassed the full area of False Bay and some of the open ocean surrounding the Cape Peninsula. Due to the very fine scale changes which occur in the coastal ocean, different grid resolutions will cause the wave dynamics to differ ever so slightly and this can affect the results which are obtained for the specific locations. It is therefore important to ensure that the simulation output of the current study are consistent between domains, and if not, to select the grid which best represents the wave dynamics and resultant conditions within False Bay. The results from the grid independence test is shown in section 4.2.3.

4. Results

4.1 Introduction

The results displayed in this section show the output obtained from the wave condition simulations calculated by the phase-averaging spectral model SWAN. These results describe the impact which rocky bank and the inherent wave properties have on the resultant wave conditions within False Bay. Five numerical wave simulations were performed (see table 3.2):

- **S1:** Realistic representation of Rocky Bank (control)
- **S2:** Rocky Bank removed at a 70 m depth
- **S3:** Rocky Bank raised and broadened to 24 m from a base of 70 m
- **S4:** Narrower directional spreading value of 22.9°
- **S5:** Broader directional spreading value of 27.6°

As discussed in chapter 3, varying wave conditions based on H_{m0}, wave direction and T_p which are known to influence the bay were used as the external boundary conditions, with the same set of condition permutations being used for all model set ups (S1 - 5). This chapter will display the results which were obtained from the SWAN simulations. For the locations of the diagnostic points, refer to figure 3.7 and table 3.1.

4.2 Initial model analysis

4.2.1 Modelled wave conditions outside of False Bay

As discussed in section 3.5.1, the experimental structure of the simulations follows the permutation of the wave diagnostics H_{m0}, T_p and wave direction which increased incrementally along the external boundary. The results were therefore indicative of these permutations and show clearly how each diagnostic affects the resultant H_{m0} at each diagnostic point. Since the experimental design of this study was to model a variety of wave conditions which could affect False Bay, an artificial time-series was produced by SWAN whereby each successive (and independent) result was plotted in a time-series fashion. However, since there was no time associated with each wave condition, the simulation iteration (1 - 990) was used to create the artificial time-series. The open ocean wave conditions that go on to propagate into False Bay were captured by the 400 m depth diagnostic point (-34.6700° S 18.3187° E) and are illustrated by figure 4.1 which shows the H_{m0} for each external boundary condition. In figure 4.1, one observes relatively uniform groupings of H_{m0}. Once these values reach and exceed 5 meters, the groupings become slightly less symmetrical and the H_{m0} increases slightly along with an increase in T_p, indicating an influence of T_p on H_{m0}. This could be linked to bottom friction as the larger, longer waves become influenced by the bathymetry. The effect of wave direction and T_p are negligible at this diagnostic point due to the open ocean exposure and the depth of the water column respectively. The data shown at this point corresponds with the external boundary conditions, indicating that the selected wave conditions have propagated toward False Bay from the external boundaries.

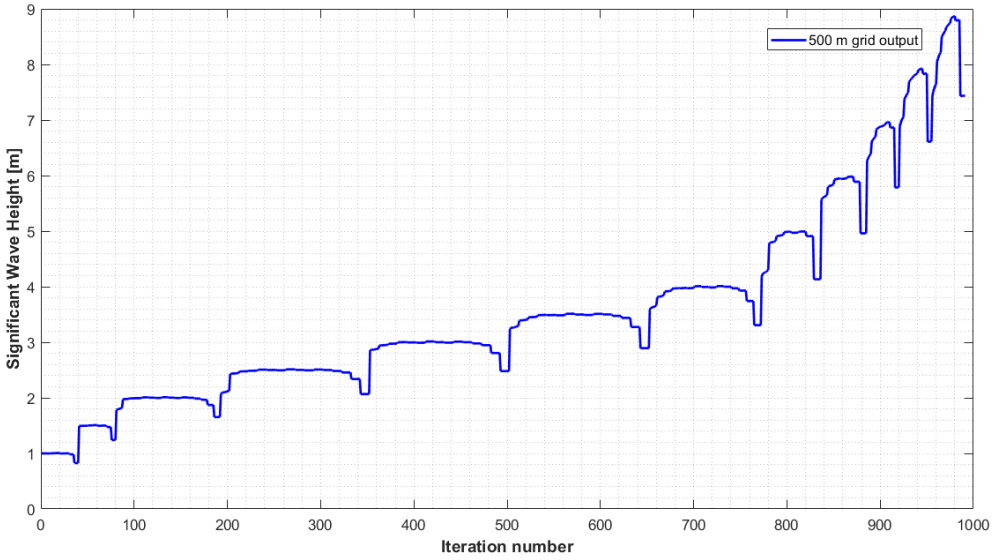

Figure 4.1: Diagnostic point located at a 400 m depth with location -34.6700° S 18.3187° E. This diagnostic point captures the wave conditions propagating towards False Bay before passing over rocky bank. The external boundary conditions were: H_{m0} (m) = 1, 1.5, 2, 2.5, 3, 3.5, 4, 5, 6, 7, 8, 9; T_p per H_{m0} ranged between 8 and 20 s while the peak wave direction for each combination of H_{m0} and T_p ranged between 180 - 270°.

4.2.2 Verification of model data

It is important to understand how a model behaves when compared to reality. Two locations within False Bay were selected where observational data was available, namely Kogelbaai (KB) and Miller's Point (MP). KB and MP are located on opposite sides of False Bay, with KB located along the eastern periphery and MP along the western periphery (see figure 3.8). The observational wave data for KB and MP was compared to that which was generated by SWAN for the same locations. Figures 4.2, 4.3, 4.4 and 4.5 illustrate how the modelled data compares to the observed data for the two locations. The statistical measures used to assess the performance of the model are described in section 3.6 with the index values shown in table 4.1.

The model simulations for the present study were based on H_{m0}, T_p and wave direction. The effect of wind was ignored (i.e. wind speeds of zero), therefore no wind-wave growth within the external boundaries could occur. Table 4.1 shows how SWAN performs better at determining H_{m0} at KB compared to MP. The study by Williams (2019) suggested that the eastern periphery

of False Bay experiences a swell dominated wave climate while the western periphery of False Bay experiences a wind dominated wave climate (Williams, 2019). Figures 4.2 and 4.3 suggest a better level of agreement between modelled and observed H_{m0} at KB (IA = 0.8350) then that which is shown by figures 4.4 and 4.5 for MP (IA = 0.5904). This corresponds with Williams (2019), since the influence of wind should have a greater level of significance at MP then at KB due to the prevailing wave climates. Since MP is situated along the wind dominated wave climate and the effect of wind was not added to the numerical experiment, the tendency for SWAN to underestimate the H_{m0} at MP is understandable (bias = -0.4657). Despite leaving the influence of wind out of the simulations, SWAN does well at estimating H_{m0} at KB. Since the wave climate at KB (and along the eastern periphery) is swell dominated (Williams, 2019) (implying that the effect of wind could be insignificant) and the modelled and observed data correspond well at KB, the external boundary conditions used in the numerical simulations for this study are appropriate for investigating H_{m0} along the eastern periphery of False Bay.

Table 4.1: Statistical measures comparing modelled and measured wave height at KB and MP

Location of diagnostic point	**Bias [m]**	**IA**	**RMSE [m]**	**SI**
KB (eastern periphery)	0.2684	0.8350	0.4156	0.2331
MP (western periphery)	-0.4657	0.5904	0.5945	0.4763

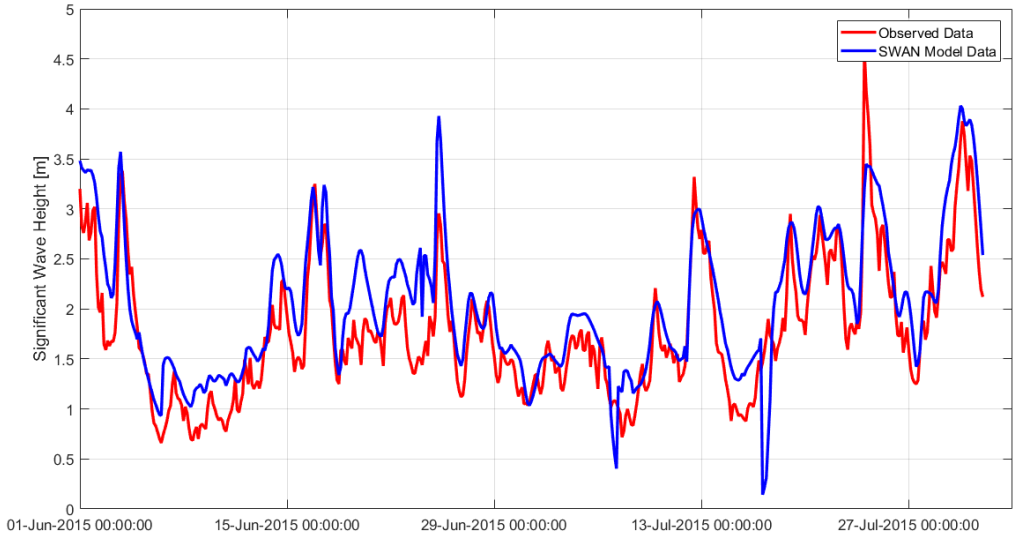

Figure 4.2: Modelled wave height data (blue) versus observed wave heights (red) shown as a time-series for the ADCP located in Kogelbaai. This point represents the area where rogue waves have been suggested to occur. This figures suggests that the model may have a slight tendency to over-predict wave heights for certain conditions.

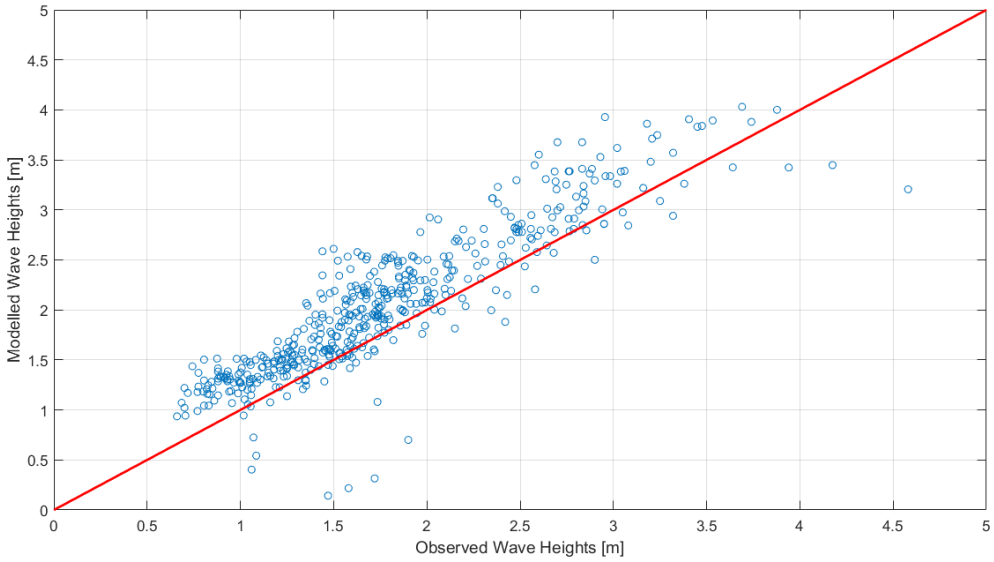

Figure 4.3: Modelled wave height data versus observed wave heights for the ADCP located in Kogelbaai. This point represents the area where rogue waves have been suggested to occur. This figure suggests that the modelled wave height data corresponds well with the wave heights recorded by the ADCP.

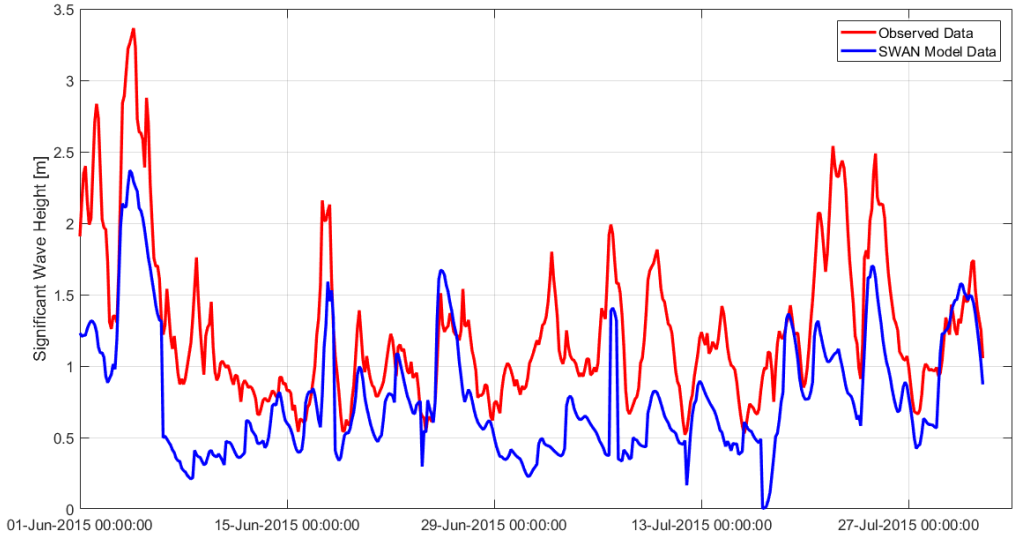

Figure 4.4: Modelled wave height data (blue) versus observed wave heights (red) shown as a time-series for the ADCP located at Miller's Point. This figures suggests that the model underestimates wave heights at MP.

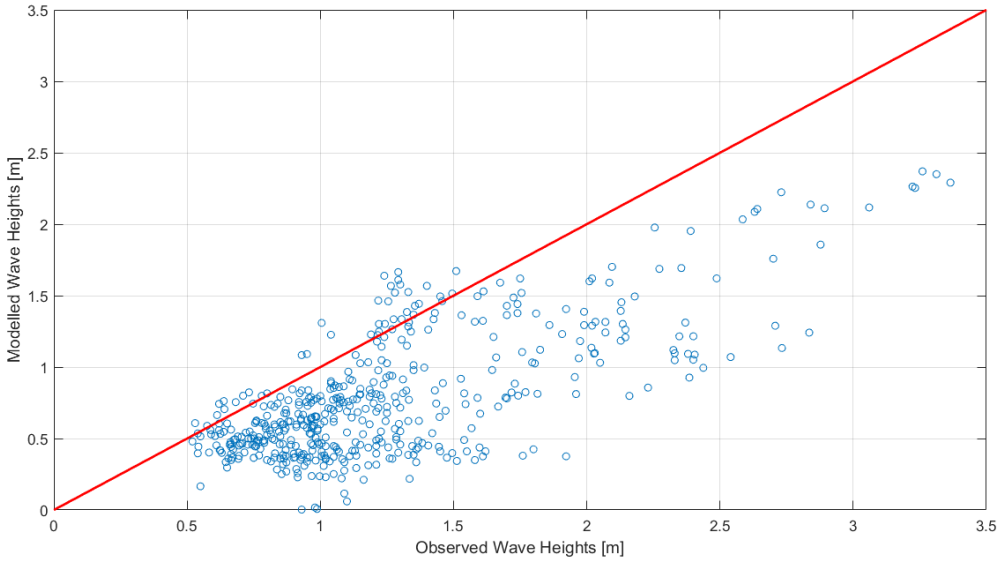

Figure 4.5: Modelled wave height data versus observed wave heights for the ADCP located at Miller's Point. This point is situated on the wind-wave dominated wave climate (Williams, 2019). This figure suggests that the model underestimates wave heights for this location.

4.2.3 Grid Independence

As mentioned in section 3.7, it was important to make use of a grid resolution which will capture the fine scale dynamics of wave propagation in shallow water. Below, figure 4.6 shows the H_{m0} for the diagnostic point at 60 m depth. At this location in False Bay (where the gradient of the sea floor is still small) the H_{m0} associated with the 500 m, 300 m and 150 m grids are similar for all wave conditions.

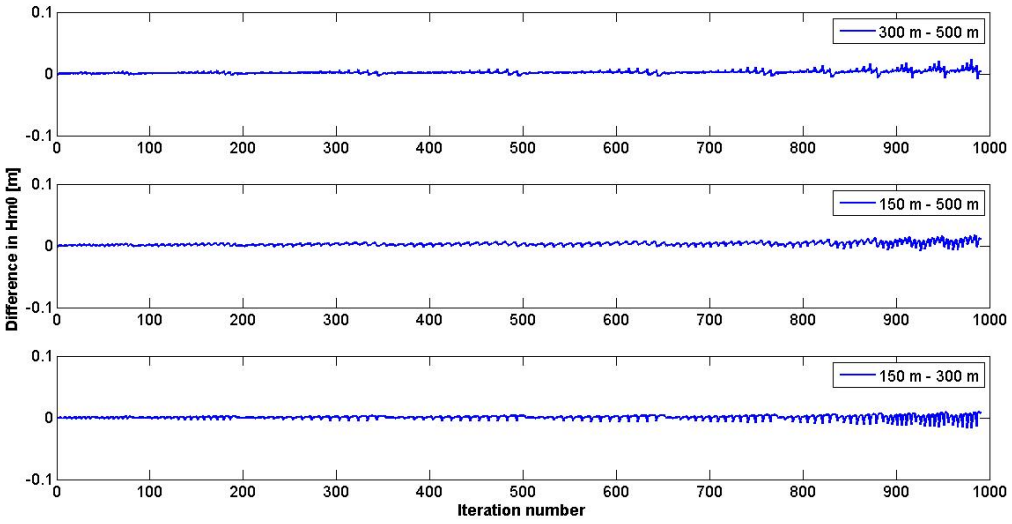

Figure 4.6: H_{m0} differences per grid observed at the 60 m diagnostic point located at -34.3038° 18.7558°. All of the H_{m0} differences are well under ±0.1 m, indicating that grids are producing very similar results.

However, figure 4.7 shows differently regarding the diagnostic points along the 20 m contour of the eastern periphery of False Bay. The H_{m0} obtained for diagnostic points 1 and 5 (locations in figure 3.1) at 20 m depths show differences in the H_{m0} obtained from each grid. The differences in the H_{m0} become more pronounced in greater, more energetic seas when the H_{m0} and T_p increase as per the external boundary conditions. These differences also become greater as one moves further south (towards point 5 - increased open ocean exposure) which is illustrated below (Note the axis limits for diagnostics points 1 and 5).

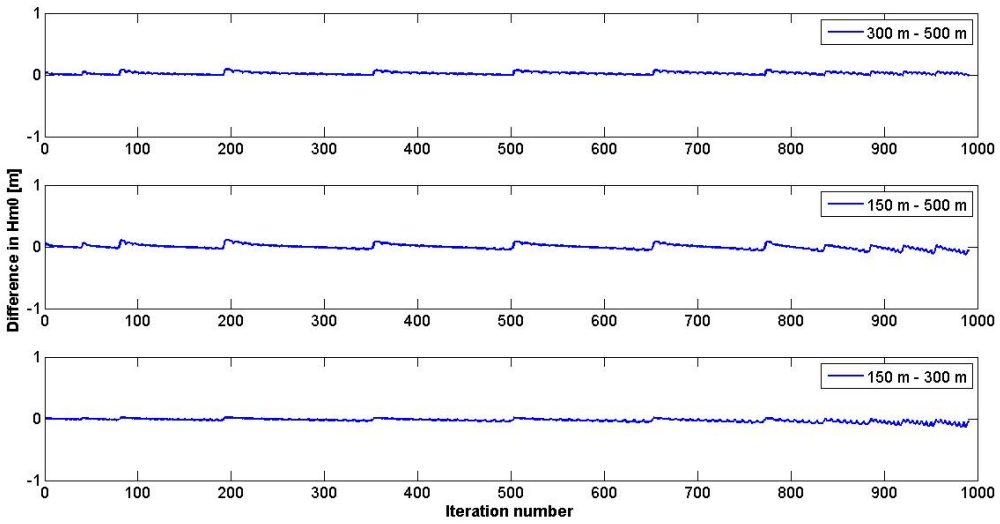

(a) Diagnostic point 1

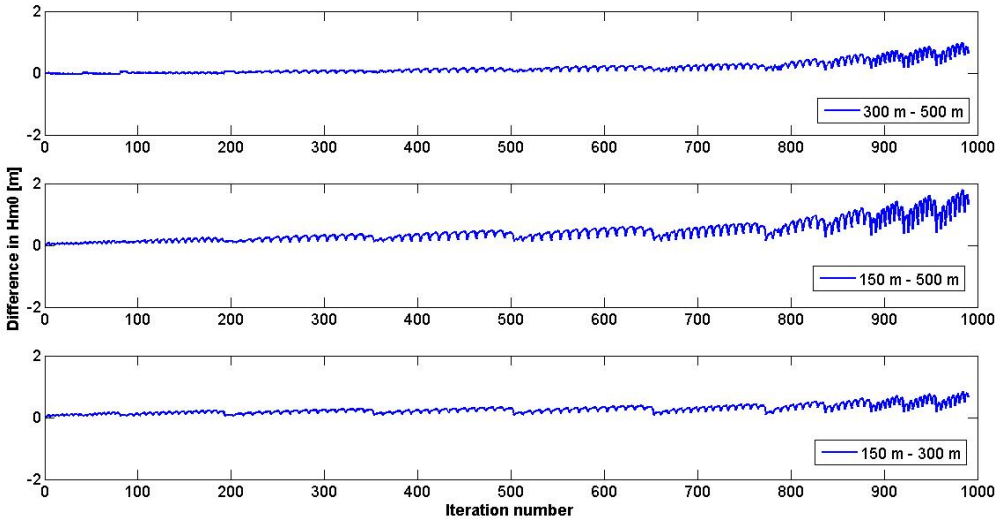

(b) Diagnostic point 5

Figure 4.7: Differene in H_{m0} between grids at diagnostic point 1 (figure 4.7a) and diagnostic point 5 (figure 4.7b). ** Note that the axis values are different for figure 4.7a and 4.7b in order to illustrate the smaller differences observed in 4.7a.

Differences in H_{m0} between grid resolutions increases towards the south. Figure 4.8 indicates the contrasting bathymetry profiles found along the northern reaches of the eastern periphery and the more southern end. The southern extent is characterized by a much steeper profile, whereas the northerly section of the eastern periphery exhibits a shallow and gradual bathymetry

profile. Figure 4.8 shows relatively well that the 150 m resolution grid captures finer details of the sea floor better than the coarser grids, especially for the steeper profile belonging to the southern extent of the coastline. These subtle topographical variations in the sea floor are important as waves in water this shallow will be influenced by the sea floor constantly, with the extent of the sea-floor's influence being related to the wavelength (which corresponds with wave period) as per linear wave theory.

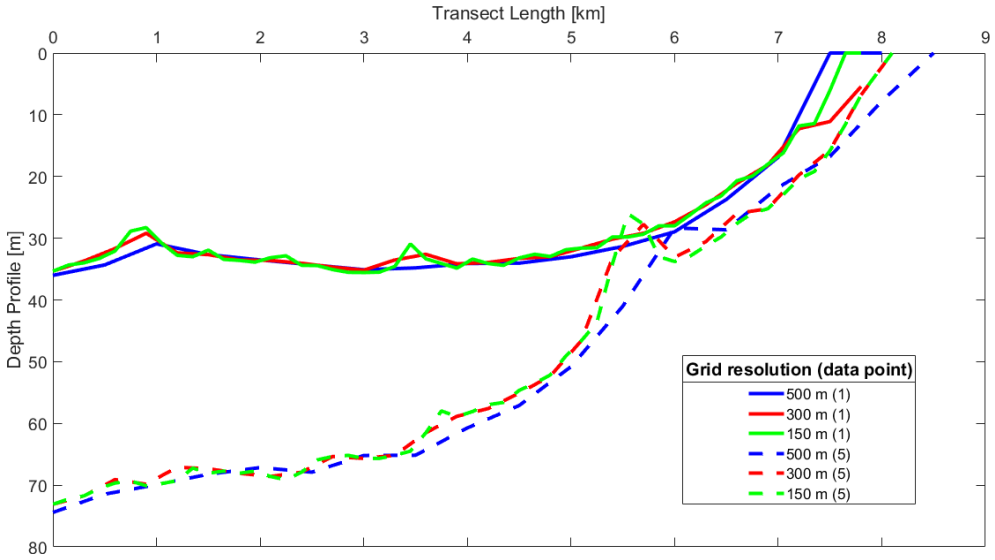

Figure 4.8: Depth profiles belonging to the southern (dashed) and northern (solid) ends of the eastern periphery of False Bay depicted at different resolutions and comparing the effect that the grid resolution has between a steep and gradual bathymetry profile extending 8 km offshore.

Figure 4.8 shows that the coarser 500 m grid does not include the small variations in the sea-floor compared to the more varied sea-floor's captured by the 150 m and 300 m resolution grids. The 150 m and 300 m resolution grids do show finer scale variability associated with the sea-floor since the bathymetry was interpolated from the depth samples over shorter distances. It was for this reason that the grid nesting technique was used. When comparing the 300 m and 150 m grids, the bathymetry profiles are not markedly different. However, looking at the H_{m0} differences in figure 4.7, the 150 m meter grid accounts for greater wave growth in the coastal region when compared to the 300 m grid. Since at this depth the waves will be impacted by the sea floor constantly (over every meter), the grid resolution for the nested grid was set to 150 m.

4.3 Wave conditions entering False Bay

According to the model results obtained from the control experiment S1, the maximum H_{m0} in False Bay was associated with external boundary conditions with wave directions between 195° for swells with larger T_p (exceeding 16 s) and 205° for more frequently occurring T_p values (i.e. those between 10 and 14 s). Figure 4.9 shows the H_{m0} at the 60 m depth diagnostic point with red asterisks illustrating H_{m0} values associated with these external boundary wave directions. The figure also suggests that the maximum H_{m0} at this location decreases for increasing T_p. This decrease in H_{m0} could be a result of energy dissipation via increased bottom friction for larger T_p swell systems.

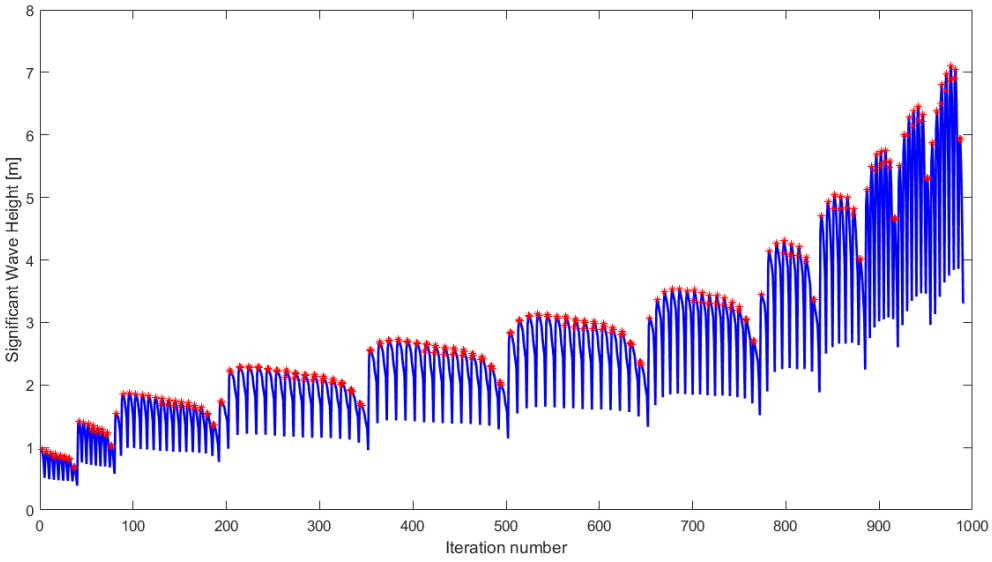

Figure 4.9: 60 m depth diagnostic point located at -34.3038° 18.7558°. The red asterisks indicate H_{m0} associated with external boundary conditions with wave directions between 190° and 210°.

4.4 Wave heights along the eastern periphery

4.4.1 Exposure to swell

The eastern periphery of False Bay displayed variability with regard to H_{m0}. Diagnostic point 1 (blue) represented the northern end of the eastern periphery and diagnostic point 10 (red)

represented the southern end of the coastline. The southern extent of the bay was clearly shown to be more exposed to the open ocean swell conditions, especially to more westerly swell, then the northern extent due to the shielding action of the Cape Peninsula. This was shown by figure 4.10 generated from the control experiment S1, which showed very clearly that the southern extent experiences greater H_{m0} then the northern sector. The influence of the Cape Peninsula on H_{m0} along the eastern periphery was also captured very well at diagnostic points 1 and 10. This is indicated by the smaller arches in the figure which illustrate sudden increases and decreases in H_{m0} as the wave directions set as the external boundary conditions change from 180° to 270°.

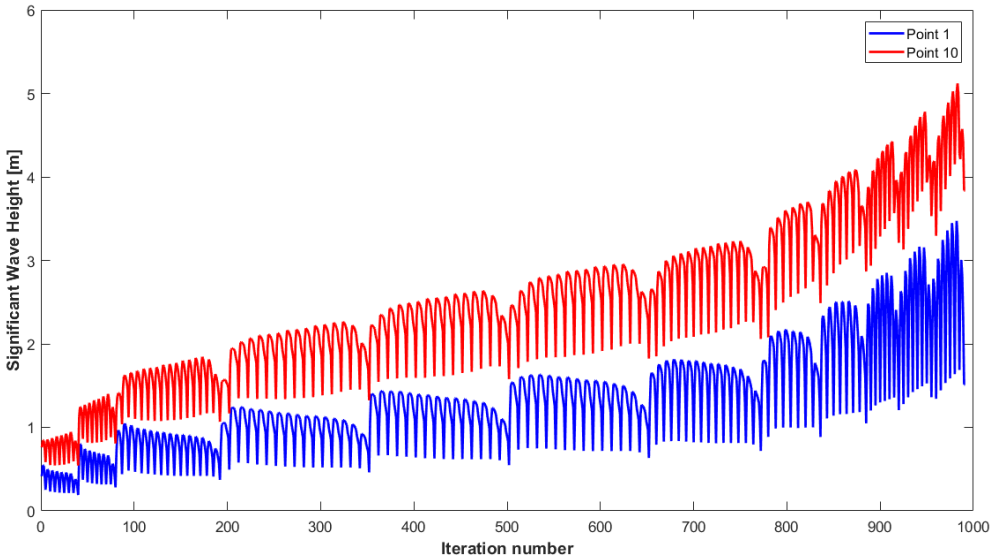

Figure 4.10: With the Cape Peninsula preventing most wave energy from entering False Bay, the southern extent of the eastern periphery (represented by diagnostic point 10 - red) has much greater H_{m0} than the northern extent of the bay (represented by diagnostic point 1 - blue).

At both diagnostic points 1 and 10 (blue and red respectively), the wave direction was shown to have a large influence on H_{m0}. Diagnostic point 1 is found in the more sheltered, gradual sloping bathymetry of the northern reaches of the eastern periphery of False Bay whereas diagnostic point 10 is located at the exposed, steep bathymetry found at the southern tip of the coastline (see figure 3.7). Smaller H_{m0} were associated with external boundary conditions with wave directions of 270° and are indicated by the lower end of each series, with H_{m0} reaching

maximums when the H_{m0} along the external boundary approaches from between 195° and 205°. These curves illustrate the effect that the Cape Peninsula has on preventing westerly wave energy from entering False Bay. The shapes of each curve show different patterns for H_{m0} and are likely to be linked to the different bathymetry profiles found at each location. The lower bound of each curve show different trends for H_{m0}. For constant H_{m0} (along the external boundary) and increasing T_p, minimum H_{m0} values increase at diagnostic point 10 and are shown to be relatively constant at diagnostic point 1. Maximum H_{m0} at each diagnostic point, which occur when swell approaches from between 195° and 205°, follow opposite trends. For the more exposed location (red), an increase in T_p causes the maximum H_{m0} to increase, whereas the maximum H_{m0} at diagnostic point 1 (blue) decrease in size with increasing T_p. Due to the varying bathymetry profiles at the two diagnostic point locations, the differences in H_{m0} may be linked to wave energy dissipation due to bottom friction. Wave energy may be constantly lost due to the shallowness and small gradient of the northern extent of False Bay and reducing the wave energy which reaches diagnostic point 1, contrasting the much deeper and steeper coastline at diagnostic point 10, where more wave energy reaches the shoreline and thus generating larger H_{m0} values.

4.5 Effect of Rocky Bank

To investigate the extent to which rocky bank can influence the wave conditions within False Bay three variations of rocky bank were generated. This section will compare experiments S1, S2 and S3. These are described in section 3.5.2.

4.5.1 Wave refraction over Rocky Bank

The shallow sea-mount's location is illustrated in figure 3.7 in section 3.4.2. Due to this variation in bathymetry, incoming wave energy will refract as it passes over the shallower region whereby increased T_p should result in greater extents of refraction as well as increased H_{m0} in the region of the rocky bank due to the waves shoaling over it. For this set of results, the control experiment S1 was used. This is depicted in figure 4.11, which shows how increased T_p along the external

boundary influences the wave conditions within False Bay with external boundary conditions of $H_{m0} = 3$ m and a 245° wave direction. Figure 4.11a shows the average wave conditions within False Bay for $T_p = 8$ s and figure 4.11b shows the average wave conditions for $T_p = 18$ s with the white vector arrows indicating the 8 s period system's resultant wave direction within the bay. It is clearly shown that increased T_p results in a greater degree of wave refraction with wave directions for the 18 s period system shown to be at a more northerly direction after passing rocky bank. This increased refraction allows more wave energy to reach the more sheltered western periphery of the bay. Also shown in figure 4.11, is an increase in H_{m0} directly after rocky bank for the larger period swell as well as a less uniform distribution of H_{m0} along the eastern periphery of False Bay. These figures suggest that the greater T_p swell system results in more variation in H_{m0} along the eastern periphery.

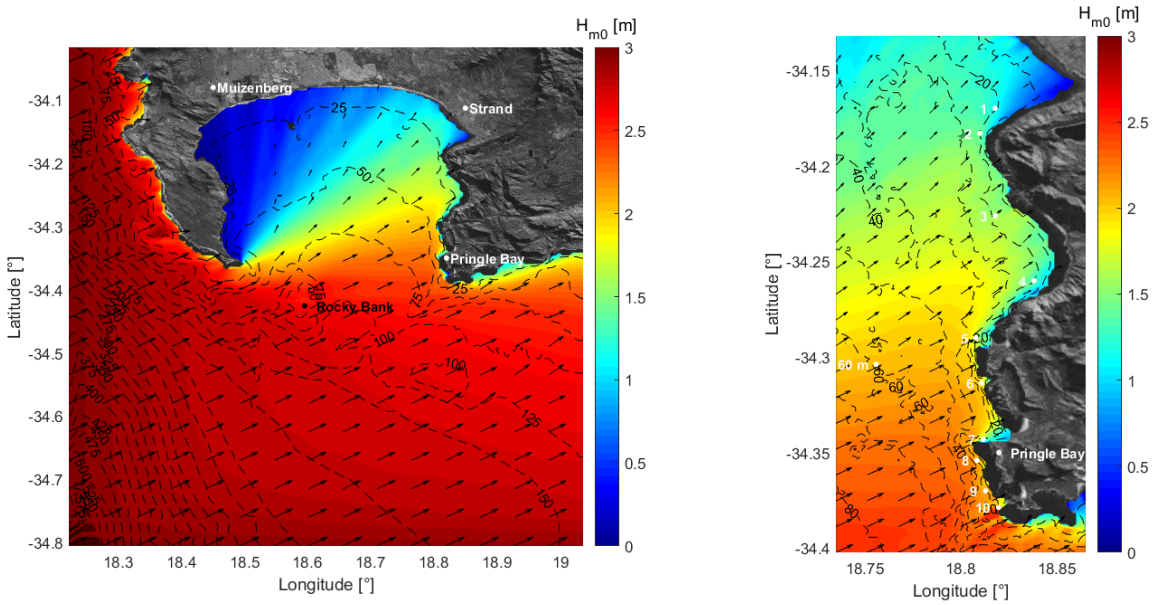

(a) Wave direction vectors with rocky bank and $T_p = 8$ seconds.

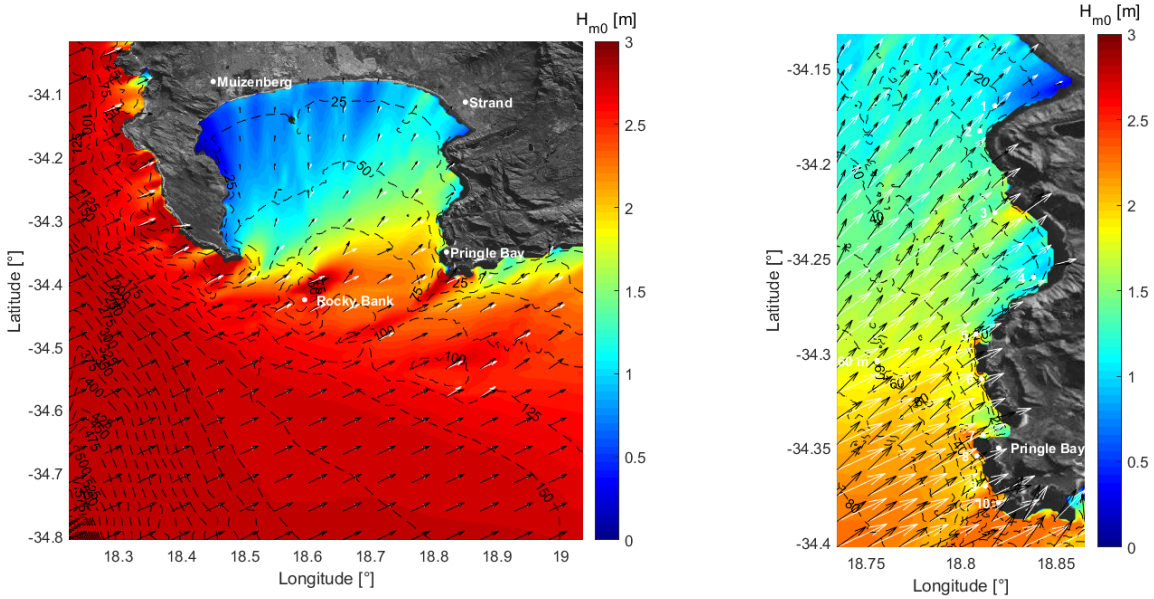

(b) Wave direction vectors with rocky bank and $T_p = 18$ seconds.

Figure 4.11: Wave direction vectors as swell passes over the area of rocky bank for external boundary conditions of $H_{m0} = 3$ m and a wave direction of 245° with 4.11a having a low T_p of 8 s and 4.11b having a large T_p of 18 s, showing white vector arrows to represent the wave directions depicted in 4.11a.

The results showing the effect of H_{m0} on wave refraction over rocky bank were taken from the

output generated by the control experiment S1. For figure 4.12, external boundary conditions were $T_p = 13$ s, wave direction = 225°, with $H_{m0} = 3$ m, 6 m, and 9 m for figure 4.12a, 4.12b and 4.12c respectively. The change in refraction patterns for increased H_{m0} were not as significant as an increase in T_p. Figure 4.12c was the only figure to show any change in wave direction due to changes in H_{m0}, which compared wave directions within False Bay between a 3 m (white vector arrow) and 9 m (black vector arrow) external boundary wave height. For constant T_p and wave direction along the external boundary, changes in H_{m0} along the external boundary have a very nominal effect on wave direction within False Bay even when increased to a 9 m open ocean swell.

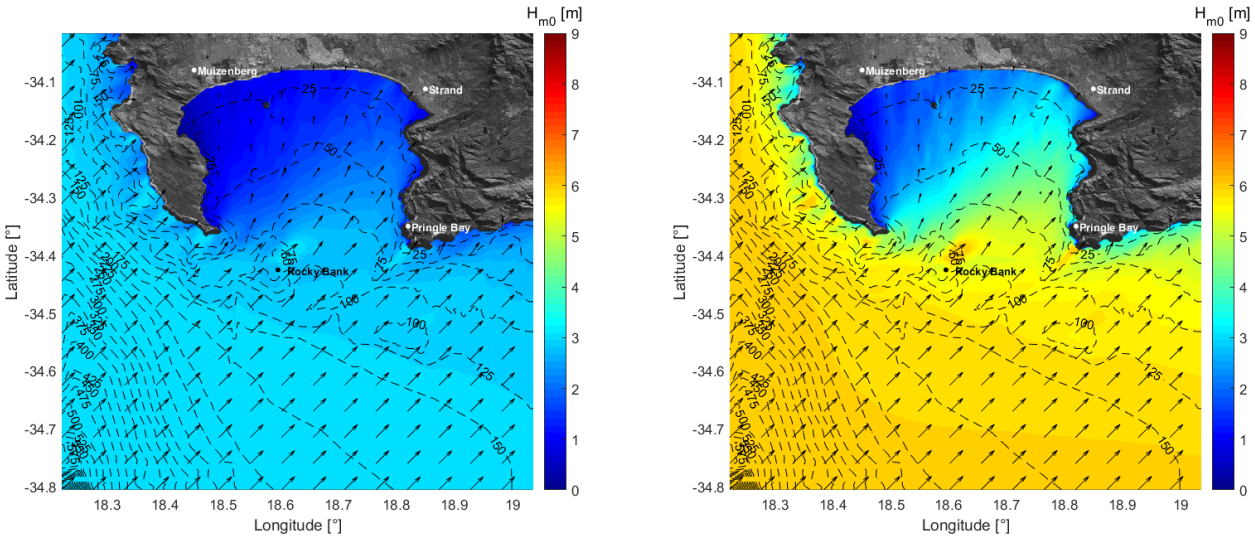

(a) $H_{m0} = 3$ meters.

(b) $H_{m0} = 6$ meters.

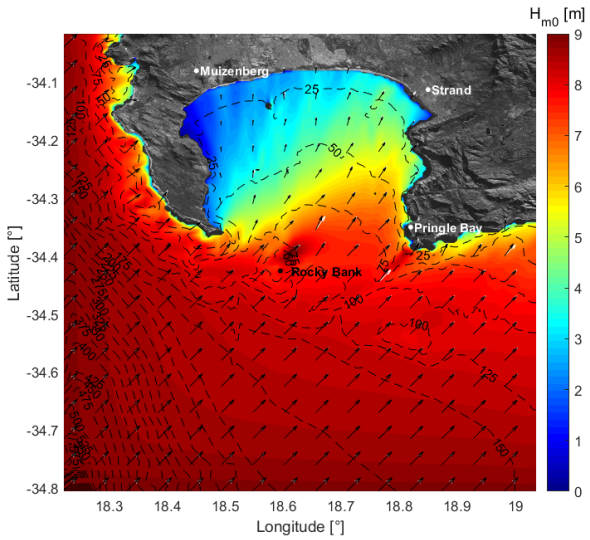

(c) $H_{m0} = 9$ meters.

Figure 4.12: Wave direction vectors as swell passes over rocky bank for external boundary conditions of $T_p = 13$ s and a wave direction of 225°. The white vector arrows in 4.12c represent the vector arrows from 4.12a.

4.5.2 Rocky Bank vs. No Rocky Bank

The first comparison between different bathymetry profiles was made between the control experiment S1 and the removed rocky bank experiment S2. The bathymetry can be compared

using figure 3.7 in section 3.4.2 and figure 4.13. Without rocky bank, the bathymetry at the mouth of the bay is consistent, therefore, one would expect no unusual wave refraction to occur over the region of where rocky bank was located.

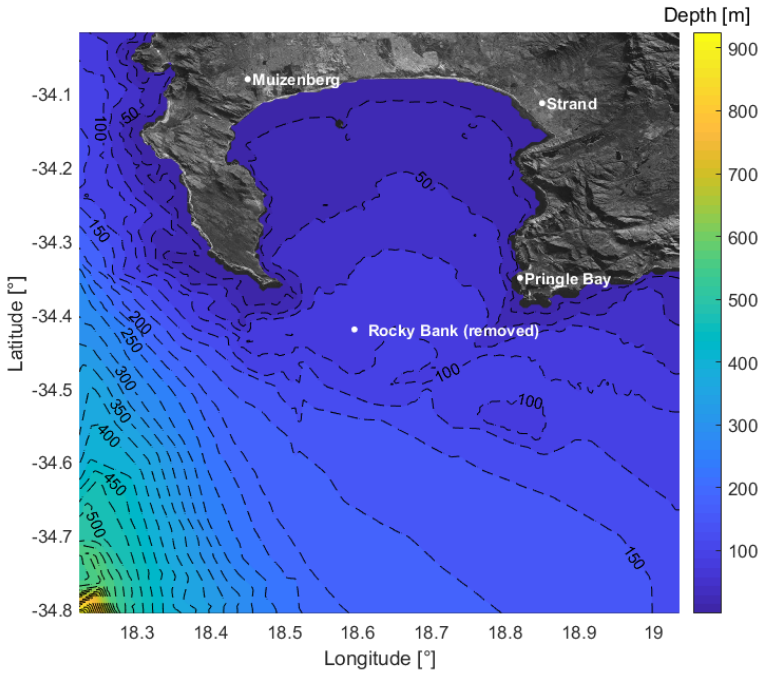

Figure 4.13: Bathymetry of False Bay where rocky bank has been removed for experiment S2. The shallow sea-mount was removed along a 70 m depth contour.

Figure 4.14 shows the change in refraction patterns occurring over the area of rocky bank for experiments S1 (4.14a) and S2 (4.14b). As expected, the removal of rocky bank at the mouth of False Bay does cause the resultant wave direction within False Bay to change. Figure 4.14b shows white vector arrows to represent the wave direction generated from experiment S1. For the specified external boundary conditions, SWAN suggests that rocky bank causes wave directions to change in a region directly behind the sea-mount. For this set of external boundary conditions where $H_{m0} = 3$ m; $T_p = 13.5$ s and the wave direction $= 225°$, the change in wave direction is small. However, since the wave direction in other parts of the bay are suggested to be unaffected, the slightly more northerly wave direction caused by rocky bank may lead to swell converging as the waves propagate toward the coastline.

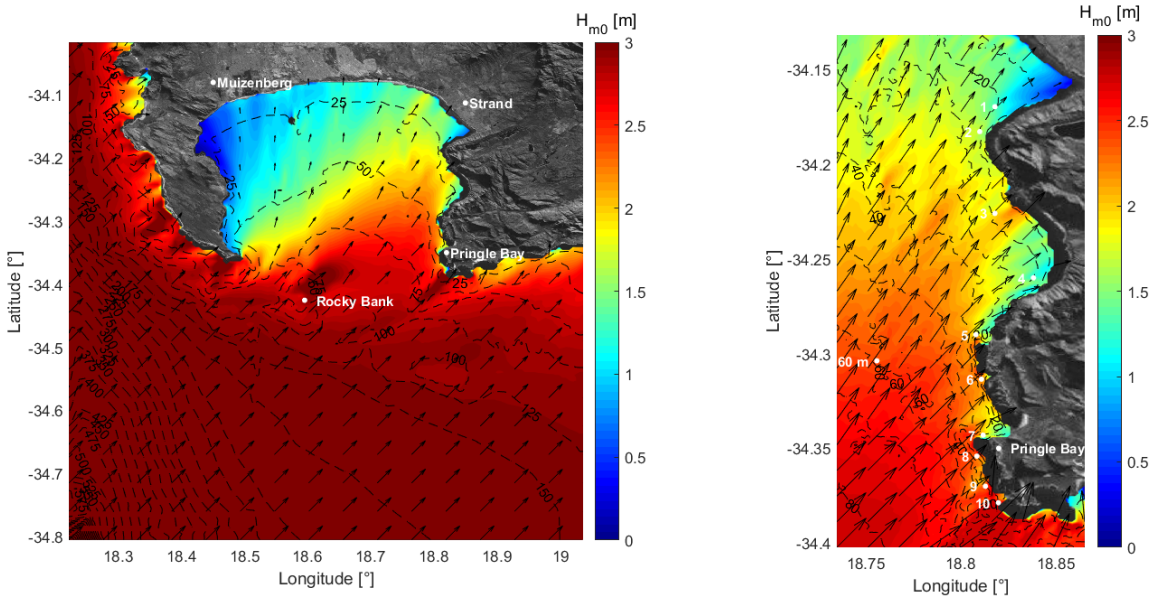

(a) Wave direction vectors with rocky bank

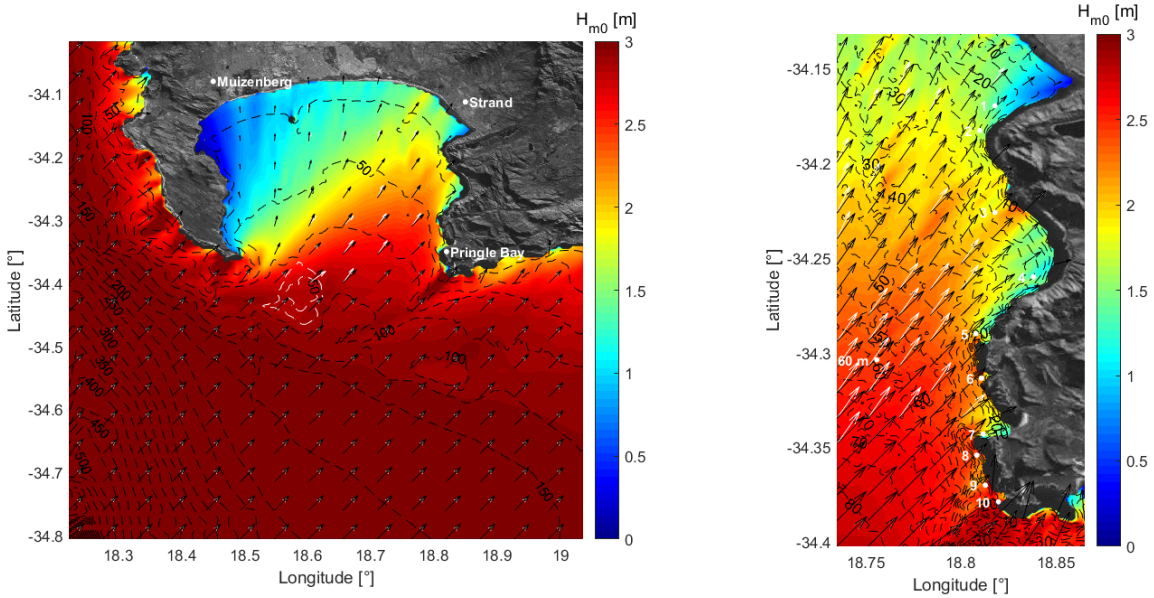

(b) Wave direction vectors without rocky bank

Figure 4.14: Wave direction vectors as swell passes over the area of rocky bank for a swell with $H_{m0} = 3$ m, $T_p = 13.5$ s and a wave direction of 225°. Figure 4.14a shows the wave refraction which occurs over rocky bank, while figure 4.14b shows no refraction when rocky bank has been removed with the white vector arrows taken from 4.14a as a comparison.

The H_{m0} anomaly plots show the difference in H_{m0} between experiments S1 and S2. The H_{m0} anomaly, for external boundary conditions of $H_{m0} = 2.5$ m, wave direction = 180° and

variable T_p, is shown by figure 4.15. The figure shows that rocky bank does influence the average H_{m0} within False Bay and appears to both refract and dissipate wave energy. These two processes, according to figure 4.15, increase and decrease H_{m0} within the bay. In figure 4.15, positive H_{m0} anomalies are indicated by red and show the extent to which rocky bank refracts the incoming swell, whereas the negative anomalies, indicated by the blue, suggest that rocky bank is reducing the wave energy which passes directly over it and thus decreasing the H_{m0} and subsequently the wave energy in these regions. The comparison made in figure 4.15 is between a 9 s and 16 s period swell. The larger period swell (figure 4.15b) leads to greater H_{m0} anomalies as well as a greater angle of refraction. This again shows that T_p has a strong influence on the wave conditions within False Bay. When analysing the effects of the external boundary wave direction, these differences, intuitively, shift around the bay corresponding to the wave direction. The directional change results in H_{m0} anomalies to occur at different parts of the coastline and is illustrated by figure 4.16.

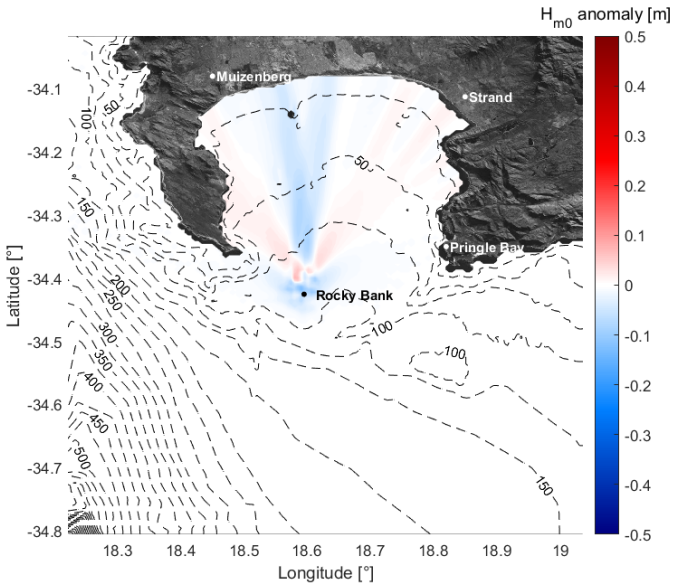

(a) $H_{m0} = 2.5$ m; $T_p = 9$ s; Dir = 180°

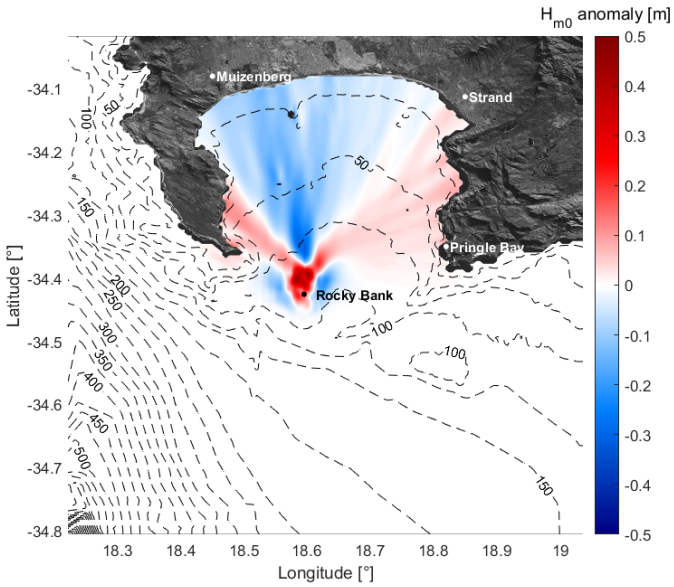

(b) $H_{m0} = 2.5$ m; $T_p = 16$ s; Dir = 180°

Figure 4.15: H_{m0} anomaly in False Bay between experiment S1 and S2. The larger T_p swell of figure 4.15b causes larger H_{m0} differences between the two bathymetry profiles while also causing a greater angle of refraction over rocky bank.

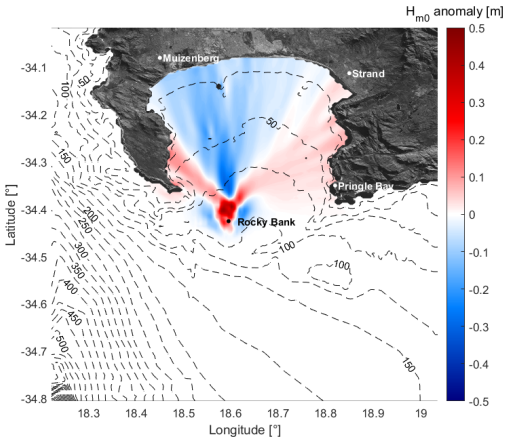

(a) Dir = 180°

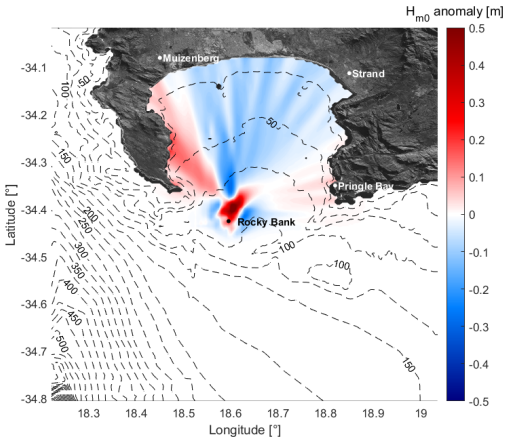

(b) Dir = 205°

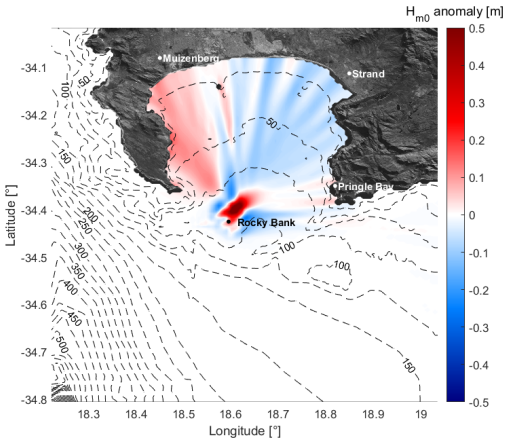

(c) Dir = 225°

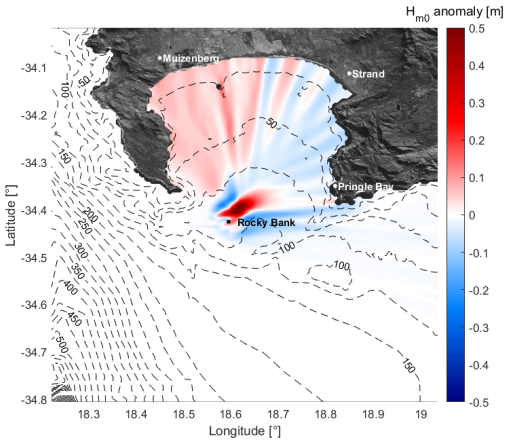

(d) Dir = 245°

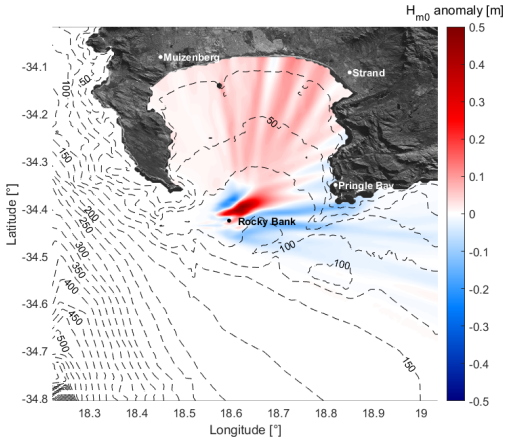

(e) Dir = 270°

Figure 4.16: H_{m0} anomaly in False Bay between experiment S1 and S2. This set of figures aims to illustrate the way in which changes in the incoming wave direction along the external boundary of constant H_{m0} and T_p (2.5 m and 16 s respectively) causes the H_{m0} anomaly to shift around False Bay.

The figures in section 4.5.2 show the H_{m0} around the area of rocky bank to be greater than the surrounding sea and especially for external boundary conditions with larger T_p. Since this is a steep and shallow bank, waves which pass directly over rocky bank will be influenced by it, the rest of the swell line which does not pass over rocky bank, will carry on to propagate in a similar direction. With rocky bank removed in figure 4.15, it is illustrated well how rocky bank increases the H_{m0} in this region. An interesting feature which is shown very clearly in the figures from figure 4.16 are the finger-like patterns associated with the positive/negative anomaly. These patterns would be associated with some form of focusing/defocussing and will be discussed further in chapter 5.

4.5.3 Rocky Bank vs. Raised and Broadened Rocky Bank

For this comparison, the control experiment S1 was compared to experiment S3 for which the 75 m depth contour of rocky bank was raised to 25 meters. This created a flatter and broader version of rocky bank. These variations in bathymetry can be compared between figure 3.7 in section 3.4.2 and figure 4.17. This adapted formation of rocky bank gives the incoming wave energy a greater surface area at a 25 m depth to be influenced by, contrastingly to the more peaked (and realistic) representation of rocky bank.

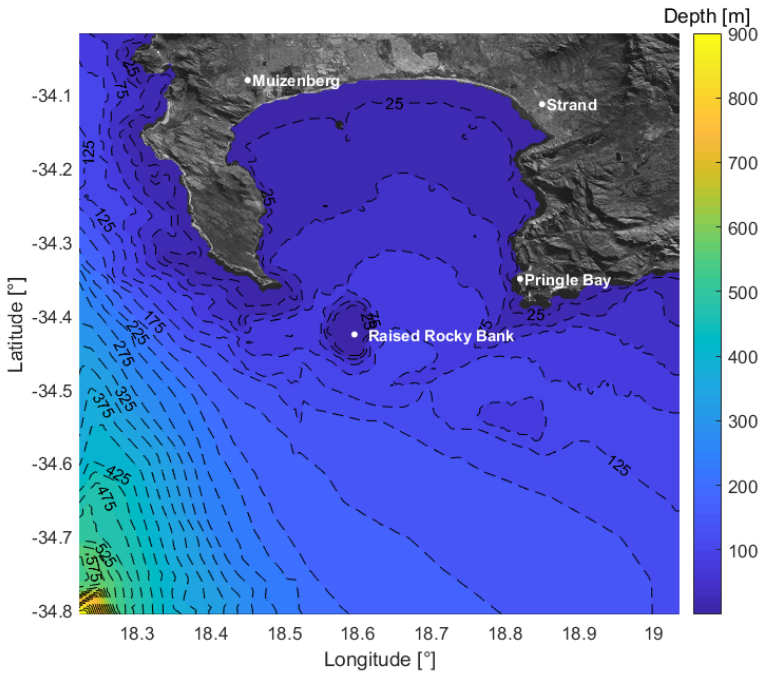

Figure 4.17: Bathymetry of False Bay where rocky bank has been raised for experiment S3. Rocky bank was raised from a 75 m depth to 25 m.

Similarly to figure 4.14, the shallowing and broadening of rocky bank does influence the wave direction within False Bay. Figure 4.18 shows the resultant wave direction within False Bay for external boundary conditions H_{m0} = 3 m, T_p = 13.5 s and a wave direction of 225°. For the comparison between experiments S1 and S3, figures 4.18a and 4.18b show the resultant conditions for experiment S1 and S3 respectively. The wave directions in False Bay do differ between the two experiments. Due to the broadness and shallowness of rocky bank in experiment S3, the wave energy approaching the eastern periphery of False Bay gets refracted over a larger surface and could cause the focusing point to move. The H_{m0} along the eastern periphery also shows to be slightly smaller in the northern section of the eastern periphery. This would be explained by increased energy loss due to the broader version of rocky bank in experiment S3. The H_{m0} anomaly plots below show the difference in H_{m0} for experiments S1 and S3. Figure 4.20 shows the difference in H_{m0} generated by the different profiles of rocky bank with external boundary conditions H_{m0} = 2.5 m, T_p = 16 s with shifting wave directions beween 180 - 270°.

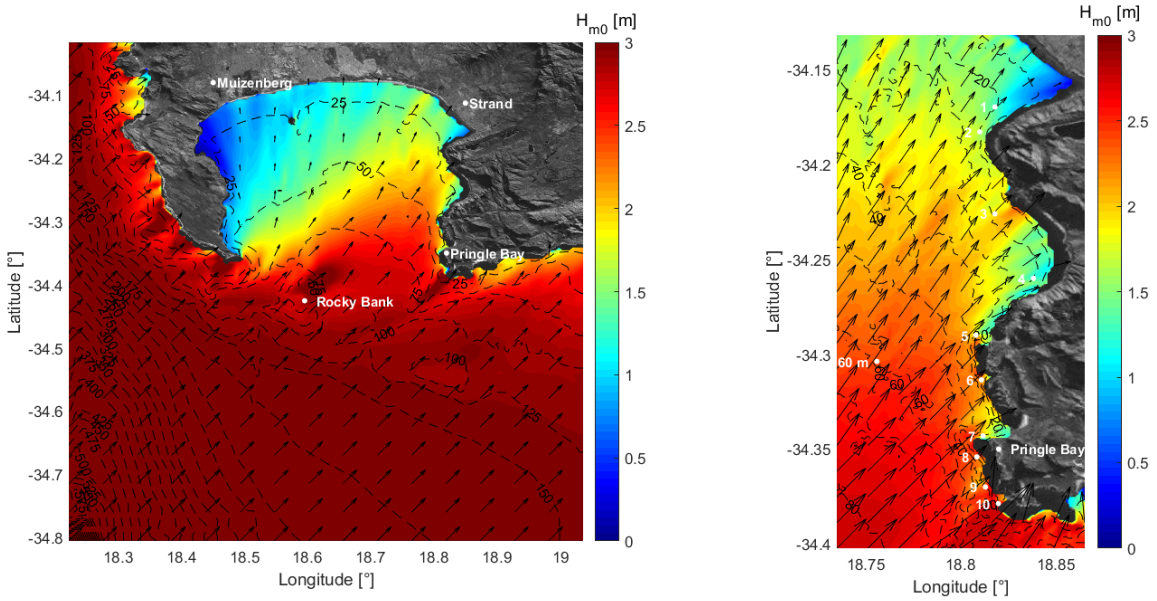

(a) Wave direction vectors with rocky bank

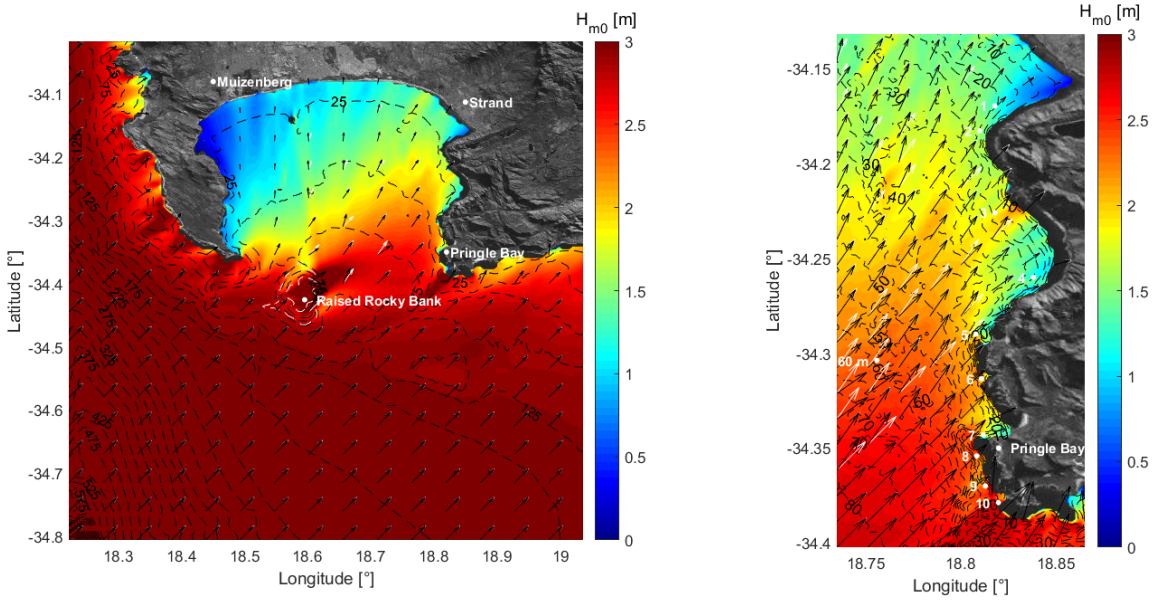

(b) Wave direction vectors with a raised rocky bank

Figure 4.18: Wave direction vectors as swell passes over the area of rocky bank for external boundary conditions $H_{m0} = 3$ m, $T_p = 13.5$ s and a wave direction of 225°. Figure 4.18a shows the effect of rocky bank on the wave direction and figure 4.18b shows what occurs when rocky bank has been raised, with white vector arrows representing the wave vectors from figure 4.18a.

Figure 4.19 shows the H_{m0} anomaly caused by changing the T_p along the external boundary with external boundary conditions H_{m0} = 2.5 m, wave direction = 180° and variable T_p. For this comparison, the positive H_{m0} anomaly (red) occurs directly behind the sea-mount and the negative H_{m0} anomaly (blue) occurs to the left and right of the prevailing wave direction. This pattern shows that the raised and broadened version of rocky bank (S3) causes smaller H_{m0} than the control version of rocky bank (S1) directly behind the shallow bathymetrical feature. Wave energy dissipation will be greater for experiment S3 and due to this, the H_{m0} directly behind rocky bank will be lower than that of experiment S1 as less energy is lost.

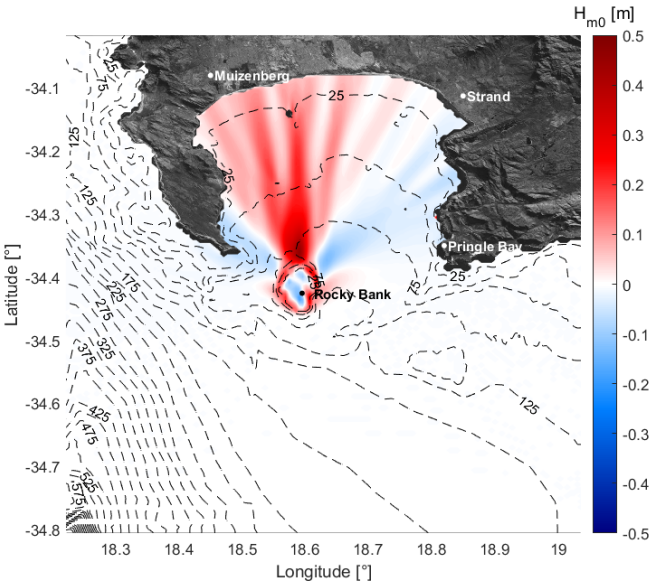

(a) $H_{m0} = 2.5$ m; $T_p = 9$ s; Dir = 180°

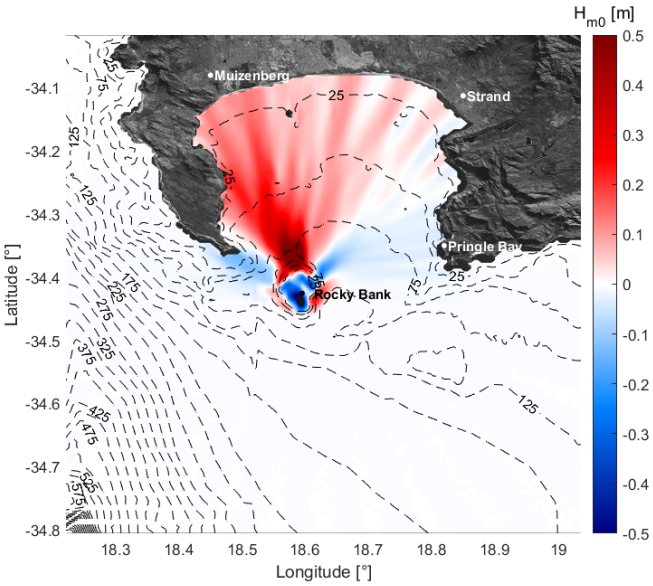

(b) $H_{m0} = 2.5$ m; $T_p = 16$ s; Dir = 180°

Figure 4.19: H_{m0} anomaly in False Bay between experiment S1 and S3. Similarly to figure 4.15, the magnitude of the anomaly is greater for the larger external boundary T_p .

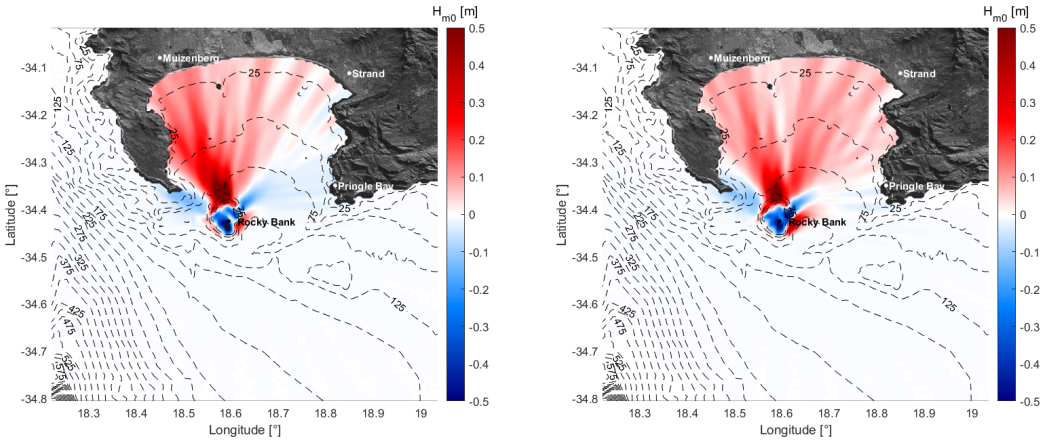

(a) Dir = 180°

(b) Dir = 205°

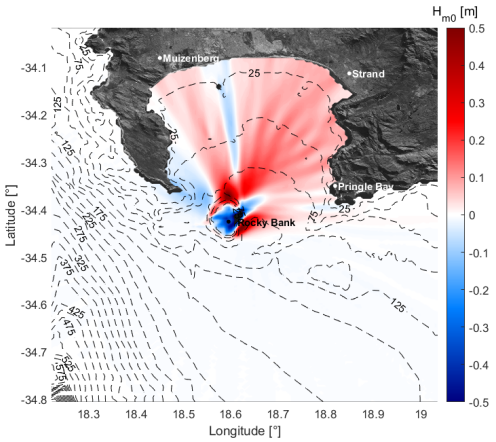

(c) Dir = 225°

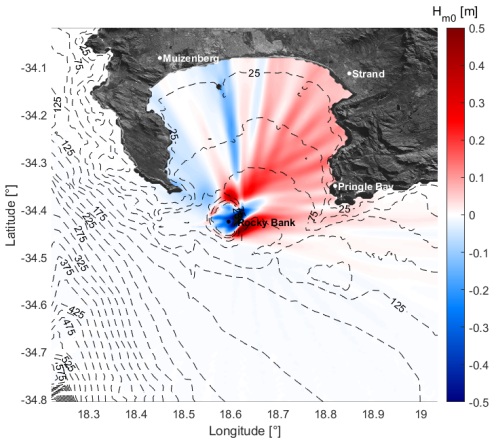

(d) Dir = 245°

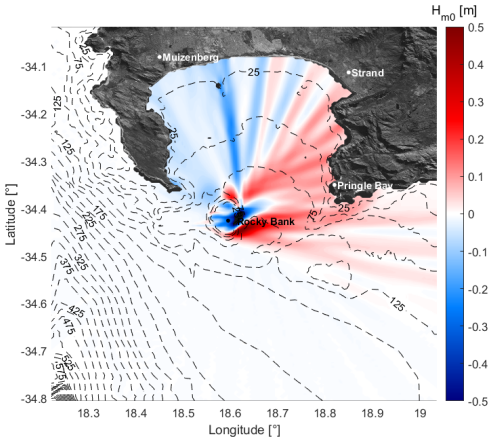

(e) Dir = 270°

Figure 4.20: H_{m0} anomaly in False Bay between experiments S1 and S3. This set of figures aims to illustrate the way in which the incoming wave direction for a constant H_{m0} and T_p (2.5 m and 16 s respectively) causes the H_{m0} anomaly to shift around False Bay.

4.6 Additional results

4.6.1 Influence of near-shore bathymetry

Diagnostic point 3 corresponds with the area where wave energy is focused, leading to the rogue wave activity as suggested by Shipley (1964), however, despite removing rocky bank (section 4.5.2), increased H_{m0} along the eastern periphery of False Bay still occurred near the location of diagnostic point 3. Figure 4.21 analyses the influence of the near-shore bathymetry along the eastern periphery of False Bay by increasing the T_p along the external boundary. The external boundary conditions used were $H_{m0} = 1$ m, a wave direction of 225° and $T_p = 8$ s and 16 s figure for 4.21a and 4.21b respectively. This result suggests that the bathymetry closer to the coastline may also be steering and focusing the incoming swell and is suggested to be more influential for increased T_p. 4.21b shows a less uniform distribution of H_{m0} along the eastern periphery, with a small area near diagnostic point 3 where the H_{m0} is larger (approximately 0.4 m) then the surrounding conditions.

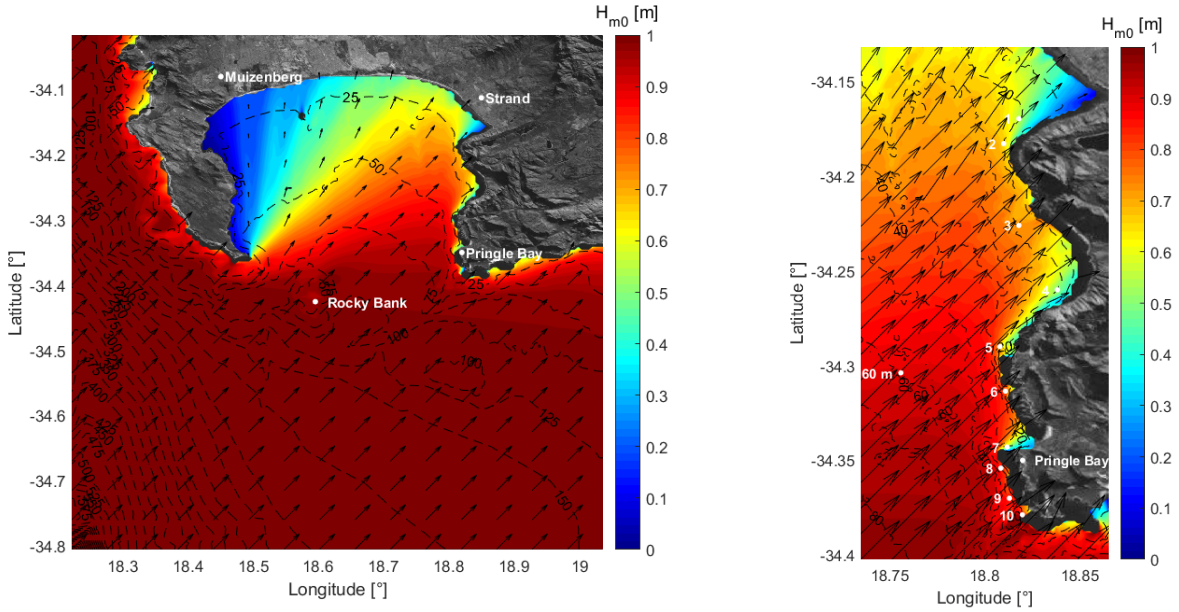

(a) Wave direction vectors with rocky bank and $T_p = 8$ seconds.

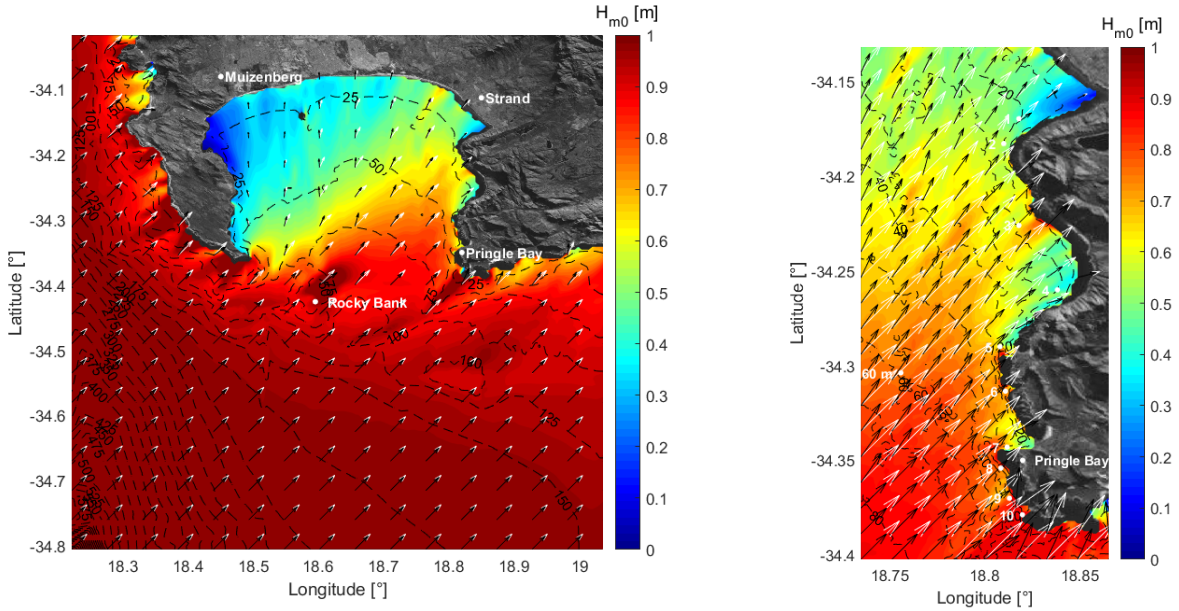

(b) Wave direction vectors with rocky bank and $T_p = 16$ seconds.

Figure 4.21: Wave direction vectors obtained from the control experiment S1 as swell passes over rocky bank. External boundary conditions were $H_{m0} = 1$ m, a wave direction of 225° and a T_p of 8 and 16 s.

4.6.2 Effect of directional spreading

To identify the effect directional spreading may have on the wave conditions within in False Bay, the directional spreading factor was narrowed and broadened along the external boundary to create experiments S4 and S5 respectively. These were then compared to the control experiment S1. The structure of these experiments is shown in table 3.2. Experiment S4 had a spreading value of 22.9° with experiment S5 having a spreading value of 27.6°. The control spreading value for the Cape Peninsula was set at 24.9°. Figure 4.22, with external boundary conditions H_{m0} = 3 m, T_p = 13.5 s and a wave direction of 225°, does not show any major difference in the overall wave conditions within False Bay. However, near diagnostic point 3, larger H_{m0} is shown to occur right along the coastline in figure 4.22a and to less of an extent in figure 4.22b. This suggests that wave systems with a narrower directional spreading factor may be more conducive to rogue wave development as the figure suggests a greater discrepancy of H_{m0} near diagnostic point 3 compared to the surrounding sea.

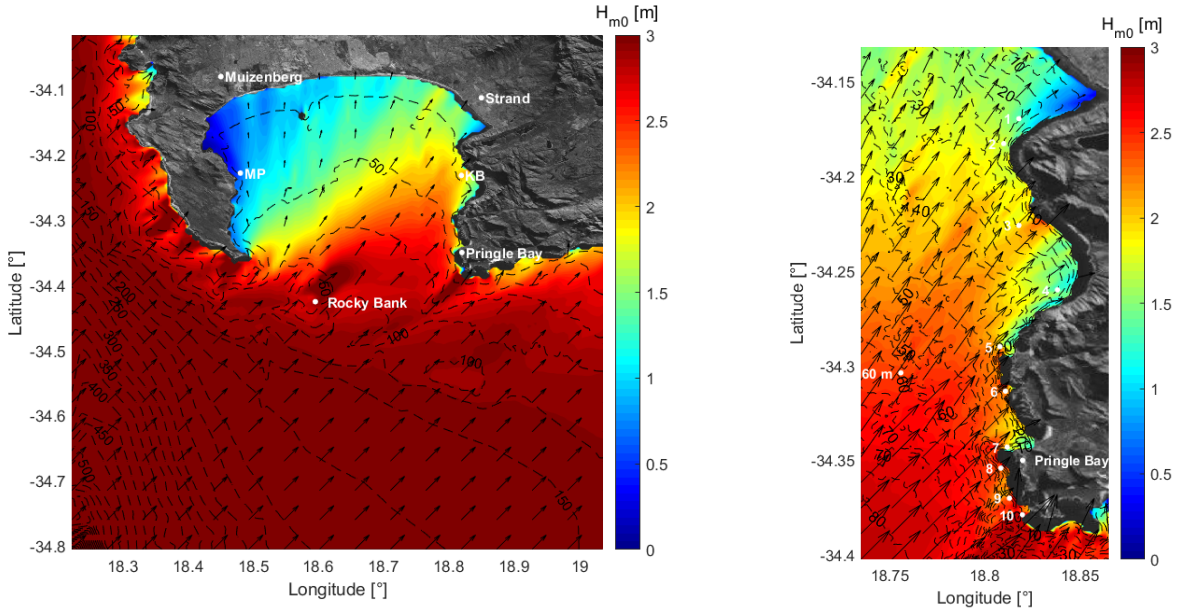

(a) Narrow spreading value: 22.9°

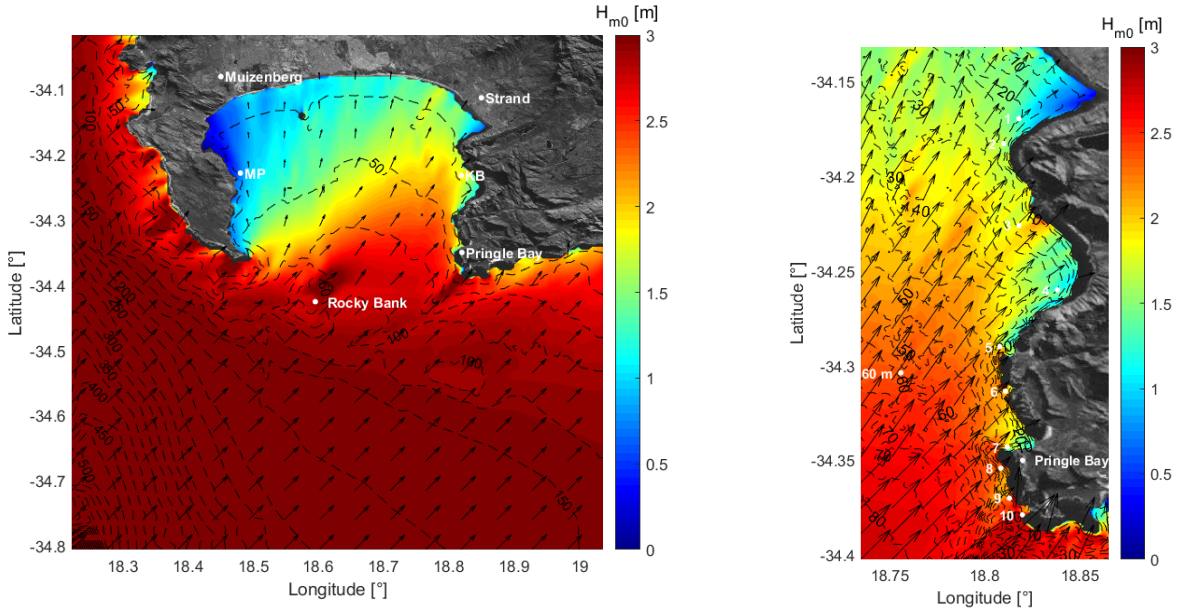

(b) Broad spreading value: 27.6°

Figure 4.22: Wave conditions in False Bay for experiments S4 (narrower) and S5 (broader). The external boundary conditions were $H_{m0} = 3$ m, $T_p = 13.5$ s and a wave direction of 225°.

Figure 4.23 shows the H_{m0} anomaly caused by changes in the directional spreading value with external boundary conditions $H_{m0} = 3$ m, $T_p = 13.5$ s and a wave direction of 225°. Figure

4.23a is the H_{m0} anomaly between experiments S1 and S4 and figure 4.23b is the H_{m0} anomaly between experiments S1 and S5, where red (blue) indicates a positive (negative) H_{m0} anomaly. In both cases, the narrower directional spreading value (for both comparisons) causes larger H_{m0} along the eastern periphery. Figure 4.23 shows that a narrower directional spreading value (S4) will result in greater H_{m0} in the direct path of the swell when compared to a wave system with a broader directional spreading value (S5). Due to the greater angle of energy dissipation for experiment S5, H_{m0} along the more sheltered western periphery of False Bay are marginally larger. The magnitude of the H_{m0} anomalies for experiments S4 and S5 are small ($\pm$0.25 m) for the 3 m H_{m0} along the external boundary.

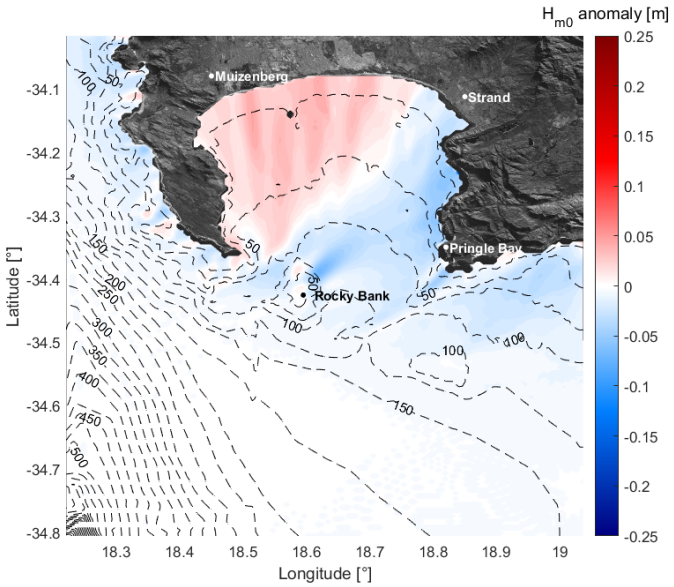

(a) Narrow spreading value: 22.9°

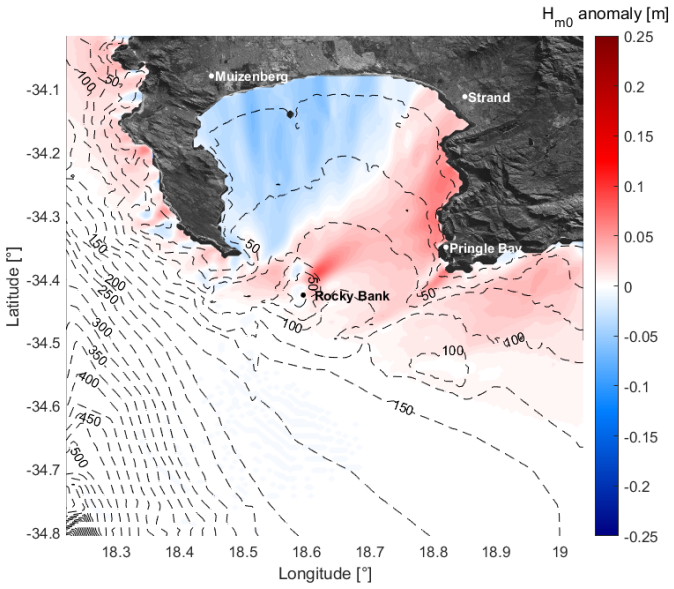

(b) Broad spreading value: 27.6°

Figure 4.23: H_{m0} anomaly due to differences in directional spreading of wave systems. Figure 4.23a compares experiments S4 and S while figure 4.23b compares experiments S5 and S1. The external boundary conditions were $H_{m0} = 3$ m, $T_p = 13.5$ s and a wave direction of 225°.

4.6.3 Wave Energy

Wave energy increases as T_p and H_{m0} increase. Figure 4.24 indicates areas along the eastern periphery of False Bay that show zones of greater wave energy for increased T_p. The external boundary conditions were $H_{m0} = 3$ m, a wave direction of 225°and $T_p = 8$ s, 11.5 s and 16 s for figures 4.24a, 4.24b and 4.24c respectively. The southern extent of the eastern periphery shows high wave energy for increased T_p, compared to the northern sector which is less energetic and comparable for smaller and larger T_p. However, in the vicinity of diagnostic point 3, is an area of greater wave energy for larger T_p (fgure 4.24c. This small zone of greater wave energy is surrounded by coastal seas with approximately half the wave energy and is suggestive of wave energy focusing.

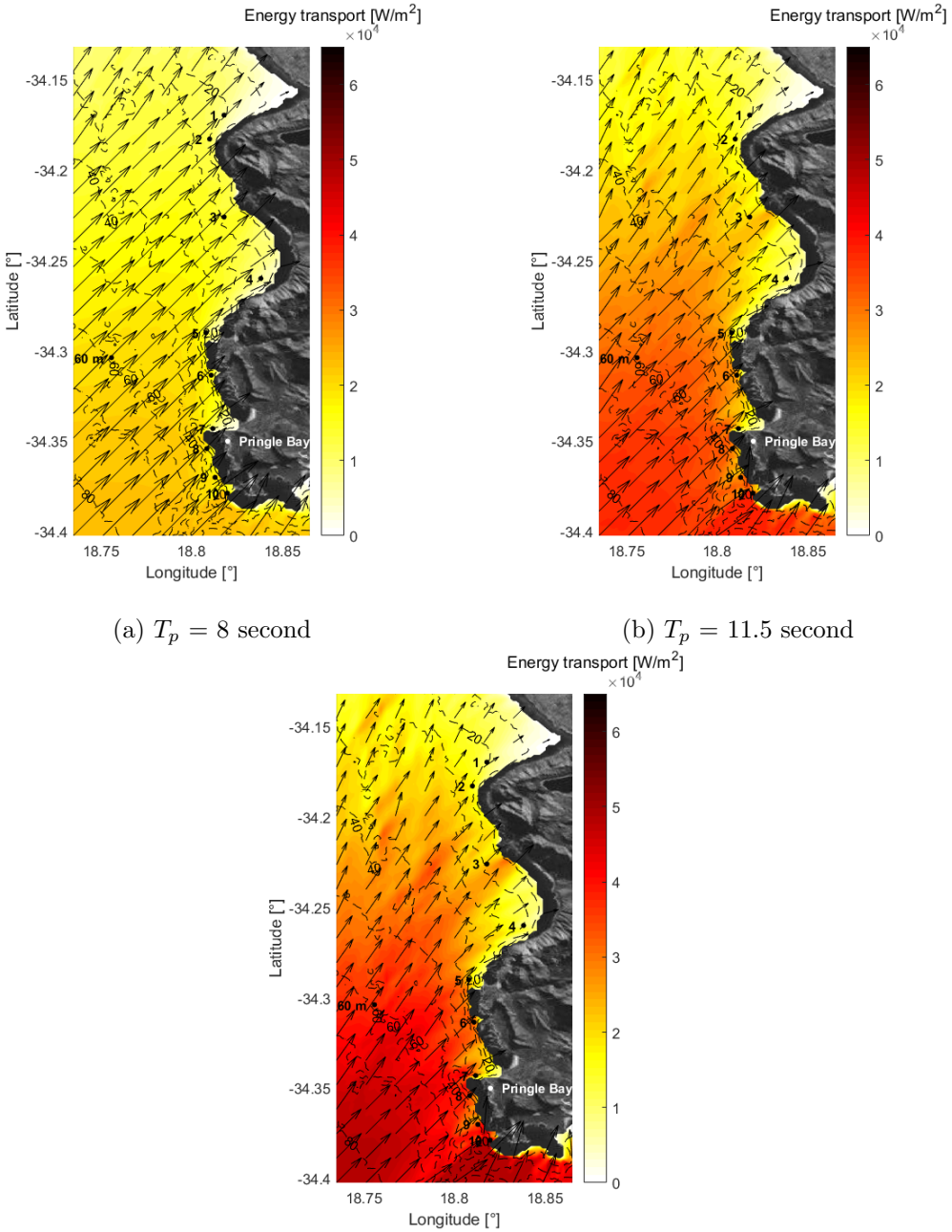

(a) $T_p = 8$ second

(b) $T_p = 11.5$ second

(c) $T_p = 16$ second

Figure 4.24: Wave energy along the eastern periphery of False Bay for increasing T_p. The external boundary conditions were $H_{m0} = 3$ m, a wave direction of 225°and increasing T_p (8 s, 11.5 s and 16 s).

5. Discussion

5.1 Introduction

False Bay, located at the southwestern tip of South Africa, is a shallow coastal embayment. Open towards the south, the bay is exposed to swell generated within the Southern Ocean. The predominant wave direction which influences the south-western coast of South Africa is 225°, which is indicative of the passing of eastward propagating mid-latitude cyclones which develop in the westerly wind belt. These mid-latitude cyclones cause the wave direction to turn more westerly when these systems pass further north in winter. The western boundary of the bay is protected from these energetic seas by the Cape Peninsula which forms the coastline of the western periphery of False Bay, whereas the eastern periphery of the bay is naturally more exposed to the the more westerly swell. This study investigated offshore wave conditions and the influence of a shallow bathymetrical feature, called rocky bank, on the wave climate within False Bay as it has been suggested to focus wave energy towards a small section of coastline along the eastern periphery of False Bay and has been suggested to be the reason for rogue wave activity in this region Shipley (1964). These rogue waves, which represent an extreme concentration of wave energy, have since been associated with the deaths of rock fishermen along this stretch of coast (NSRI, 2019), who get swept off the rocks by these much larger waves ($H_f \leq 2H_{m0}$). To capture the influence of rocky bank on the wave climate of False Bay, the standard wave diagnostics used to describe a wave climate (H_{m0}, T_p and wave direction) were manipulated to form a range of wave conditions which could influence False Bay (section 3.5.1). These values for the wave diagnostics were taken from a hind-cast time-series generated using NCEP WW3 reanalysis and served as the external boundary conditions for the simulations. This dataset

spanned a 30 year period from 1979 and 2010 and therefore gave a good indication of the average and extreme wave conditions known to occur around the Cape Peninsula. This dataset also showed the seasonality in the wave climate of the south-western coast of South Africa which is dictated by the equatorward shift of the eastward propagating mid-latitude cyclones during austral winter months (May - July). These synoptic systems generate more energetic seas during these months and are characterized by greater T_p, H_{m0} and a more westerly swell direction, compared to the lower T_p, smaller H_{m0} and more occurrences of southerly wind swells during the austral summer months (November - January) (section 2.2.1.1). The monthly climatology depicted in figure 3.2 and the directional wave roses in figure 3.3 illustrated the seasonality for each wave diagnostic clearly and gave a good understanding of the wave climate which is observed around the Cape Peninsula.

Having developed a general understanding of the wave climate around the Cape Peninsula, external boundary conditions were established which were then used to initiate the simulations run using the numerical model SWAN. Wave conditions ranging between the extreme conditions according to the NCEP dataset were selected at varying intervals, with smaller intervals between wave diagnostics which fell within the more commonly occurring conditions (see table 3.2). The monthly climatology indicated that H_{m0} between 2.5 m and 3.4 m and T_p between 11.7 s to 13.1 s were the average wave conditions which tend to occur around the Cape Peninsula during austral summer and winter respectively. As these waves propagate into False Bay from the predominantly south-westerly direction, wave energy is spatially focused by rocky bank towards various sections of the eastern periphery of False Bay (Shipley, 1964). The sea-mount rises from a depth of approximately 70 m to roughly 25 m and is relatively conical in shape (as depicted by the SWAN depth profile in figure 3.7). Due to this variability waves will be refracted and, as theorized by Shipley (1964), will be focused towards the eastern periphery of False Bay. This spatially induced focusing concentrates wave energy and is a reasonable explanation for the occurrence of rogue wave development within False Bay. This investigation will use the range of conditions provided by the NCEP WW3 reanalysis time-series in order to better understand the effect which rocky bank has on the resultant wave conditions within the bay, particularly

rogue waves. To begin understanding the influence which rocky bank has on the wave conditions within False Bay, two manipulations to rocky bank were made to be compared with SWAN's depiction of rocky bank. One where rocky bank was removed to a 70 m depth (experiment S2), decreasing as much of the variation in the sea floor as possible and the second where rocky bank was raised to a 25 m depth (experiment S3) with the peak of the sea-mount also being broadened.

This study set out to characterize which wave diagnostic is most influential in leading to the suggested rogue wave activity along the eastern periphery of False Bay, South Africa. Due to the shallow sea-mount at the mouth of False Bay, incoming wave energy will undergo refraction as swell passes over the shallow bathymetry. According to linear wave theory, the depth at which a wave begins to be influenced by the sea-floor is when the depth is less than or equal to half of the wavelength. This lead to the expectation that the T_p of a wave system will be most influential in rogue wave development since the refraction patterns caused by rocky bank will become more significant as this wave diagnostic increases. Not only should greater T_p result in an increased extent of spatial focusing, but should also result in greater exceedances of the rogue wave threshold criterion. This section will now critically analyze the results from chapter 4, discussing the impact which the wave diagnostic permutations and the manipulations of the shallow bathymetrical feature called rocky bank had on the resultant wave conditions within the bay in an attempt to conclude which open ocean conditions (in this case the external boundary conditions), which propagate into False Bay, may be conducive for rogue wave occurrence along the eastern periphery of False Bay.

5.2 Importance of this study

Rocky bank was suggested by Shipley (1964) to be responsible for increased wave heights and rogue waves along the eastern periphery of False Bay. This coast has been nicknamed the 'Death Coast' due to the many drowning incidents which have occurred amongst coastal users, particularly in the rock fishing community. These incidents have been attributed to rogue waves which catch the anglers off guard and wash them off of the rocky coastline, with the

most recent incident having occurred on the 15^{th} June 2019 (NSRI, 2019). Logically, these fishermen would be less likely to go out to the coastline during extreme wave conditions and would therefore take advantage of the dangerous coastline during conditions which appear calm during which the shoreline is more accessible. The recent study by de Vos & Rautenbach (2019) investigated the relationship between various types of coastal incidents and coastal marine weather in South Africa, aiming to quantify the extent which the safety of coastal marine activity is affected by by severity of the weather. de Vos & Rautenbach (2019) categorized three weather types; *Good*, *Marginal* and *Bad*. These classifications were based on visibility, wave height and wind (more details can be found in de Vos & Rautenbach (2019)). With the "wave conditions" being pertinent to the present study, the three weather categories described above were grouped according to the following wave height ranges: $<$ 2 m (*Good*), 2 - 3 m (*Marginal*) and $>$ 3 m (*Bad*). The general feeling within the coastal user communities showed that if any single diagnostic was considered to be bad (wind or wave height or visibility), that the overall conditions be classified as *bad* (de Vos & Rautenbach, 2019), therefore one can say that big waves and energetic seas ($>$ 3 m) would be classified as bad weather. This wave height falls within the average seasonal H_{m0} range for the Cape Peninsula (approximately 2.5 m - 3.4 m), which shows that the south-western coast of South Africa is exposed to *bad* marine coastal weather (de Vos & Rautenbach, 2019). de Vos & Rautenbach (2019) classified four coastal activity types: group 1 included swimmers and bathers; group 2 included the likes of surfers, paddlers, windsurfers, etc; group 3 included light vessels while group 4 included large scale ships such as trawlers and fishing vessels. de Vos & Rautenbach (2019) developed a simple risk map for different coastal sites around South Africa with the Cape Peninsula being one of the four sites. The risk map showed that users were most at risk during *good* conditions, with the risk decreasing as the coastal marine weather worsened (the same was the case for the other study sites). This information is incredibly useful for the present study. One would logically expect rock fisherman (and most coastal users in group 1 activities) to avoid coastal areas during bad weather conditions and therefore lowering the associated risk (de Vos & Rautenbach, 2019). This is critical to keep in mind when considering incidents regarding rogue waves. Due to their nature, these waves, which carry a significantly greater amount of wave energy than the wave

system in which the rogue wave was born, can catch even the most experienced coastal user off guard in good conditions. Understanding the conditions which may be conducive to rogue wave development is important to understand even in small seas, since any unexpected event, even if its only a knee high rogue wave in calm seas, can be fatal to any coastal user.

5.3 Rocky bank

Waves lose energy as they propagate through shallowing water columns via bottom friction and ultimately wave breaking. Due to rocky bank's shallow bathymetry (see figure 3.7), wave energy was expected to be reduced by the bathymetrical feature due to wave breaking and increased bottom friction. To illustrate rocky bank's effect on H_{m0} within False Bay, simulation output between S1 and S2 were compared. H_{m0} anomalies in figure 4.15 show clearly that H_{m0} within False Bay in direct alignment with the wave direction would be marginally greater (approximately 0.1 - 0.3 m greater) for experiment S2, and slightly greater H_{m0} (approximately 0.1 to 0.2 m) at angles to the left and right of the prevailing wave direction for the control experiment S1. This shows some indication towards wave refraction by rocky bank with wave refraction being the process whereby variable bathymetry (and/or current fields) bends and redirects incoming swell as it propagates through the area of variability. According to linear wave theory, longer wavelength waves (waves with greater periods) will be refracted to a greater extent than shorter period waves. This is also illustrated in figure 4.15 which shows the effect of increased T_p on the H_{m0} anomalies in False Bay for the comparison between experiments S1 and S2. As expected, an increased T_p causes the magnitude of the anomaly to be greater, with H_{m0} differences being less than ± 0.1 m for a 9 s period swell compared to ± 0.3 m differences when the T_p was increased to 16 s. The H_{m0} anomaly plots do not explicitly show the extent of the angle of wave refraction which occurs because of rocky bank, but figure 4.15 does indicate, via the angle of the positive H_{m0} anomaly, that the angle of refraction is increased when the T_p is increased. However, this investigation is based on the spatial focusing effect which rocky bank has on incoming swell as suggested by Shipley (1964), which can be better understood by analyzing the wave vector arrow figures from section 4.5.

Unfortunately, the output from SWAN does not allow for wave ray plots to be produced, such as the hand-drawn diagram by Shipley (1964) (figure 2.1) which would show clearly whether the incoming swell was focused towards the coast or dispersed throughout the bay. To be able to discern any possible focusing effect which may be caused by rocky bank, the wave direction vectors for different simulations were overlaid to see how different wave diagnostics influence the refraction patterns (i.e. S1 and S2 in figure 4.14). This technique shows the difference in wave direction when the wave diagnostics are changed (i.e. H_{m0}, T_p or the rocky bank profile). The effect of the wave direction along the external boundary does not influence the resultant H_{m0} along the coast, but it does result in different areas of False Bay to become more or less exposed with more westerly swells causing smaller H_{m0} along the northern sector of the eastern periphery as the shielding of the Cape Peninsula becomes more prominent. SWAN showed that the Cape Peninsula shields False Bay from most swells that have a wave direction greater than 245° with these swells only affecting the more southern areas of the eastern periphery (i.e. Rooiels/Pringle Bay). The wave direction along the external boundary associated with the greatest H_{m0} in the area which Shipley (1964) proposed wave focusing to be at its greatest (diagnostic point 3 - see table 3.1) are wave directions between 215° - 225°. When the swell direction turns to a more southerly direction and approaches from less than 205°, H_{m0} along the eastern periphery begin to decrease and H_{m0} along the northern reaches of the bay begin to increase. The only wave diagnostic that plays a significant role in influencing the wave refraction caused by rocky bank is the T_p. Figure 4.12 shows very little change in wave direction when increased H_{m0} are set along the external boundary, with a negligible change in wave direction becoming noticeable when comparing a 3 m and 9 m external boundary H_{m0}. When comparing the wave direction vectors, there was a noticeable change in wave direction after rocky bank when the T_p was increased. This is illustrated by figure 4.21 which compared a T_p of 8 s and 16 s with a 1 m H_{m0} and a wave direction of 225° as the external boundary conditions. It is clear that the external boundary conditions with the larger T_p of 16 s (figure 4.21b) was influenced to a greater extent by the bathymetry than the shorter 8 s period external boundary condition. This result, showing that increased T_p causes a significant change in wave direction after passing

rocky bank whereas an increase in H_{m0} causes very little change, supports the expectation that the T_p of a wave system has more influence on wave refraction and possible wave focusing by rocky bank.

Having showed that T_p is likely to be the primary parameter leading to changes in wave refraction over rocky bank, the actual effect of rocky bank was analyzed by comparing the different manipulations of rocky bank to the control version of rocky bank (S1). These manipulations consisted of a bathymetry profile where rocky bank was completely removed from a 70 m depth contour creating experiment S2 and a raised and broadened version of rocky bank where the peak of the sea-mount was much flatter and wider creating experiment S3. As mentioned earlier in section 5.3, rocky bank causes a marginal decrease in wave energy within False Bay due to energy dissipation processes such as bottom friction and wave breaking, becoming more prominent during larger seas (with respect to H_{m0} and T_p) . Even though this decrease is slight, wave conditions within False Bay may appear calmer than one physically observes, especially during longer period swells with smaller wave heights. To be able to discuss any form of spatial focusing caused by rocky bank one needs to analyze refraction patterns.

Figure 4.14b shows the refraction caused by rocky bank. The white vector arrows show rocky bank's influence from experiment S1 and the black vector arrows show the resultant wave direction for the bathymetry profile without rocky bank (experiment S2). For figure 4.14b, a typical swell that influences the Cape Peninsula was plotted, with external boundary conditions being a 3 m H_{m0}, a 13.5 s T_p and a wave direction of 225°. It is clear that rocky bank causes swell which passes on the east (west) side of rocky bank to be refracted to a more northerly (easterly) direction than without rocky bank. This convergence of vector arrows for experiment S1 shows that the wave energy may be converging as a result of wave refraction caused by rocky bank. This convergence of wave energy is suggestive evidence for spatial focusing. As the wave converges in on itself, wave energy which was spread becomes concentrated, which upon arrival along the shallow coastline, could shoal and grow to a height which classifies the wave as a rogue wave. Despite changing the wave direction, the area to which rocky bank redirects the swell is

still focused towards the same stretch of coastline, which is the same zone where Shipley (1964) suggested rogue wave activity due to spatial focusing via rocky bank.

5.4 Nature of Rogue Waves

Rocky bank, the shallow bathymetrical feature at the mouth of False Bay, has been shown to cause changes in wave direction due to wave refraction as the predominantly south-westerly swell propagates from the open ocean into False Bay. The numerical model SWAN suggests that the extent of wave refraction by rocky bank increases for greater values of T_p, however, due to SWAN being a phase-averaging spectral model, individually occurring rogue waves were not identifiable. Given that rogue waves are defined commonly by the rogue wave threshold criterion (where, $H_f > 2H_{m0}$), it is important to suggest that, since rogue waves in False Bay have been identified to occur in relatively small, localised areas, the H_{m0} of this smaller area of coastline should be that which is used as the threshold value. For a 1 m external boundary H_{m0}, the average H_{m0} of 40 simulations at diagnostic point 3 (varying in T_p and wave direction), was 0.549 m (this value corresponds with an observation Shipley (1964) made of 0.6 m when physically observing waves at the same location for a 1 m open ocean forecast). Therefore, it would essentially be incorrect for a rogue wave to have to exceed 2 m when the wave climate within False Bay is naturally not as great as the open ocean. Therefore, a seemingly meager wave height of 1.18 m would be enough to classify a wave as a rogue wave for a 1 m open ocean swell. Now, the method for rogue wave development in False Bay has been suggested by Shipley (1964) to be spatial focusing by rocky bank at the mouth of False Bay, which this study also supports. This rogue wave development process alone, which focuses wave energy towards sections of the coast after analyzing wave direction vectors in section 4, may not be the only process leading to extreme wave heights along the eastern periphery. In reality, a sea-state tends to consist of a primary and secondary system, if not even a tertiary swell. These swells will differ slightly in their characteristics as they will have been generated by different synoptic conditions. As indicated by 4.21, wave systems of greater T_p will be refracted at a greater angle than smaller T_p swells which also tend to approach the coastline at a more westerly and

southerly direction respectively. Not only do the wave directions begin to differ after having passed over rocky bank (causing waves to cross paths and interfere with one another), but the speeds at which the wave systems travel are different, with the longer T_p systems traveling faster than the slower, shorter T_p swells. This difference in wave speeds could result in instances where the faster waves overtake the slower wave system, which could lead to dispersive focusing. As stated in section 2.3.2.2, when the faster and longer T_p waves overtake the slower and shorter T_p waves these two systems could, momentarily, contract to fewer wavelengths (Dysthe *et al.*, 2008). It is therefore possible that there may be two mechanisms causing rogue waves to develop in False Bay. In addition, the study by Touboul *et al.* (2006) suggested that wind generated surface currents have the potential of extending the time for which the wave exceeds the rogue wave threshold criterion, as well as causing a slight increase in wave amplitude. Given that the south-westerly swell is the prominent swell direction and the south-westerly wind direction has been classified as one of the wind regimes known to influence the Cape Peninsula, it is possible that this extension of time for which the rogue wave meets it's criterion (as well as the focusing point being shifted closer to the coast), could increase the likelihood for the rogue wave to focus close enough to the coast and eventually break along the rocks.

5.5 Conclusion

Following the early study of Shipley (1964), this is one of the first studies investigating the wave climate, let alone rogue waves, in False Bay, South Africa. Shipley (1964), who did not have the power of numerical models, was able to conclude sufficiently well regarding the effect which rocky bank has on spatially focusing swell towards sections of the eastern periphery of False Bay. This study agrees well with the early study by Shipley (1964) and proposes that spatial focusing may not be the only mechanisms leading to rogue waves in False Bay and that dispersive focusing may be another mechanism causing rogue waves to occur along the eastern periphery of False Bay, South Africa. Since different wave systems, especially those which differ in wave period, will have different refraction patterns, the area toward which they are focused could differ, resulting in rogue waves to occur anywhere along the easter periphery of False Bay

from the Strand area to the southern extent of Cape Hangklip. The area which Shipley (1964) proposed as the area of most concern, is the only area within the nested grid domain to have a significantly larger wave height than its immediate surrounding and is illustrated in figure 4.21 and also shown by the wave energy plot by figure 4.24. This is the precise zone where Shipley (1964) suggested that rocky bank focuses swell and suggests that this area could be the most likely area to experience rogue waves, as it also appears that there is further focusing and concentration of wave energy by the near shore bathymetry which was analyzed in section 4.6.1.

In conclusion, it was not entirely possible to discern which conditions rogue waves were more likely to develop in using a phase-averaging model, like SWAN, as it is not possible to track individually occurring waves since the output of the model are the resulting average conditions from the specified external boundary conditions. However, conditions which become conducive to rogue wave formation are somewhat identifiable. Firstly, any rogue wave occurring in False Bay should not be compared to the significant wave heights for the open ocean conditions which propagate into False Bay, but should be compared to the typically smaller and calmer seas which occur in False Bay to; 1) more accurately characterize an extreme wave as a rogue wave according to the rogue wave threshold criterion where $H_f \leq 2H_{m0}$; and 2) to better represent their occurrence statistics, as this will allow for some form of risk index to be developed specifically for False Bay if rogue waves in False Bay are further studied in a statistical manner. One would say, based on the risk index produced by de Vos & Rautenbach (2019), that rogue waves become a greater threat during relatively calm seas. This is not only due to the increased level of human exposure, but swells with long wave periods are refracted and focused to a greater extent than low period swells and also carry a significant amount wave energy that, if coupled with other waves, may easily wash unsuspecting people along the coast into the rocky waters. From this study, the largest rogue waves, and possibly most frequent, would be expected to occur along the eastern periphery for primary wave directions between 215° - 245°, with the likelihood of a rogue wave to most likely increase if a secondary swell is propagating at a similar wave direction but traveling at a slower speed. Due to the increased refraction and greater wave energy, large wave periods ($>$ 13 s) would also be classified as being prone to rogue wave development and

that they become even more likely when a lower period (< 13 s) swell is present due to the coupled effect of spatial and dispersive focusing. In closing, this study has provided further evidence that the eastern periphery of False Bay is prone to rogue waves due to spatial, and possible dispersive, focusing mechanisms caused by rocky bank and the prevailing wave climate. Not only was this suggested by Shipley (1964), but reports of rock fishermen being washed off rocks along the Kogelbaai coastline by rogue waves (NSRI, 2019) is strong physical evidence that supports the occurrence of a rogue wave.

5.6 Implications

It is important that this information is relayed to the public especially to those who make use of high risk areas. Awareness regarding the danger of rip currents, sharks and strong waves are found at popular beaches and coastal locations around South Africa. However, it is not easy to raise awareness about events which many people may not believe to occur due to the calm conditions during which it is possible for them to occur. Raising awareness around rogue waves, especially in higher risk areas such as the eastern periphery of False Bay (as well as any coastal area exposed to waves), is vital, since even amongst the more experienced community of rock fishermen and coastal users, a few seconds could be the difference between life and death. To counter this, warning signs informing people about the possibility of rogue waves during any sea state, should be placed at locations along the eastern periphery of False Bay. Not only do physical signs need to be placed, but marine forecasts could be accompanied by a rogue wave warning based on the location of the report. Lastly, despite increasing the knowledge about the wave climate of False Bay, especially with regard to rogue waves, I hope that the this information will raise awareness about these extreme waves along the rocky coastline of of False Bay and reduce the frequency of these unfortunate incidents which have occurred along it's aptly named 'Death coast' .

Appendix A

SWAN simulation set-up

For simple uses of SWAN, wave simulations can be set up through a graphical user interface in which the user may specify the necessary parameters. By doing so, the user generates a wave input file (".mdw" file). This GUI has multiple tabs from which the wave conditions, physical parameters and grids can be specified. Below, the necessary steps and options chosen for creating and setting up the simulation conditions are described. If a section from the GUI is not mentioned, it was unused. It is important to note that the completed '.mdw' file was run using a 'wavecon' file due to the number of wave conditions which needed to be simulated since only one condition can be specified in the GUI. For further information, please see the DELFT3D-WAVE user manual (Delft3D-WAVE, 2014).

WAVECON file

In order to be able to run many successive wave conditions, as was the case for the current study, the 'wavecon' file method was used. This methodology allows SWAN to iterate through a list of wave conditions and completes the computation of many wave conditions in one simulation. The wavecon file must be found in the same directory as the '.mdw' file which was generated via the GUI. The wavecon file must be named "wavecon.rid", where '.rid' is the "run ID" (the name) of the '.mdw' file. To run a simulation using a wavecon file (or any SWAN wave simulation), one must select Wave (standalone) -> Start. This will ask for a '.mdw' file to be selected. Once the file has been selected, SWAN will automatically search for the wavecon file in the same directory and will begin to iterate through the various conditions. Note that the working directory needs

to be selected (this can be chosen at the bottom of the menu page) in order for the '.mdw' file to run. The wavecon file requires the following parameters (refer to Delft3D-WAVE (2014) for wavecon structure):

- Itdate [min] – point in time after reference date
- H_{m0} [m] – significant wave height
- T_p [s] – Peak period of energy spectrum
- Dir [°] – Mean wave direction
- ms [-] or [°] – Directional spreading (cosine power or degrees)
- Water level [m] – water level over entire model and is measured positively upward from the same datum from which bottom levels were taken.
- Wind speed [m.s^{-1}] – wind velocity 10 meters above sea level
- Wind direction [°] – wind direction 10 meters above sea level

Grids

The grids generated from the SWAN 'RFGRID' menu option are imported into the simulation under this tab. For each computational grid which is imported, under the 'Grid data' heading, the bathymetry data (created for each computational grid) can be associated with the computational grid. The nested grids are imported in the same fashion as the main grid and will automatically be nested within the main grid. The spectral resolution and hydrodynamic tabs were left unchanged.

Timeframe

This section needs one dummy time input in the time point for WAVE computation box. The rest of the time-points were added within the '.mdw' file as text. The number of timepoints is equivalent to the number of wave conditions which will be simulated.

Boundaries

The grid boundaries for the main grid are described in this section. It is important to add boundaries for all of the grid edges (even those which waves are exiting the grid from) otherwise the sudden difference in boundary conditions creates an unrealistic sea state. The boundaries, defined by their orientation (North, East, South and West) were given uniform conditions based on Significant Wave Height (m), Peak period (s), Directional spreading (degrees) and the wave direction (degrees). The wave spectra are also input as dummy variables since the values are obtained from the 'wavecon' file.

Physical Parameters

In this section the physical parameters are set. This encompasses the constants, wind, processes and various other physical processes associated to waves. The method used to model bottom friction was set to Madsen et al. White-capping is selected by default using the Komen et al. computation.

Output Parameters

In this section the locations for the model output is specified. It is necessary to check the boxes for each computational grid which is used. In SWAN, points within the study area were positioned within the area of interest.

List of Figures

List of Tables

Bibliography

Advisian. 2018. *Desalination Project: Monwabisi Outfall - Brine Dispersion Modelling Study.* Tech. rept. Advisian, South Africa.

Akhmediev, N., Soto-Crespo, J. M., & Ankiewicz, A. 2009. How to excite a rogue wave. *Physical Review A*, **80**(4).

Atkins, G. R. 1970. Thermal structure and salinity of False Bay. *Transactions of the Royal Society of South Africa*, **39**(2), 117–128.

Battjes, J. A., & Janssen, J. P. F. M. 1978. Energy loss and set-up due to breaking of random waves. *Coastal Engineering Proceedings*, **1**(16).

Bitner-Gregersen, E. M., & Toffoli, A. 2012. On the probability of occurrence of rogue waves. *Natural Hazards and Earth System Sciences*, **12**(3), 751–762.

Booij, N., Ris, R. C., & Holthuijsen, L. H. 1999. A third-generation wave model for coastal regions: 1. Model description and validation. *Journal of Geophysical Research: Oceans*, **104**(C4), 7649–7666.

Chabchoub, A., Hoffmann, N. P., & Akhmediev, N. 2011. Rogue wave observation in a water wave tank. *Physical review letters*, **106**(20), 204502.

de Vos, M, & Rautenbach, C. R. 2019. Investigating the connection between metocean conditions and coastal user safety: an analysis of search and rescue data. *Safety science*, **117**, 217–228.

Delft3D-WAVE. 2014. Delft3D-WAVE User Manual.

Dufois, F., & Rouault, M. 2012. Sea surface temperature in False Bay (South Africa): Towards a better understanding of its seasonal and inter-annual variability. *Continental Shelf Research*, **43**, 24–35.

Dysthe, K., Krogstad, H. E., & Müller, P. 2008. Oceanic Rogue Waves. *Annual Review of Fluid Mechanics*, **40**(1), 287–310.

Engineers, U. A. C. O. 2002. Coastal engineering manual. *Engineering Manual*, **1110**, 88.

Fedele, F., Brennan, J., De León, S. P., Dudley, J., & Dias, F. 2016. Real world ocean rogue waves explained without the modulational instability. *Scientific reports*, **6**, 27715.

Grundlingh, M., & Rossouw, M. 1995. Wave Attenuation in the Agulhas Current. *South African Journal of Science*, **91**(7), 357–359.

Grundlingh, M. L. 1994. TOPEX/Poseidon observes wave enhancement in the Agulhas current. *AVISO Altimeter Newsl*, **3**.

Guo, Q., & Xu, Z. 2011. Simulation of deep-water waves based on JONSWAP spectrum and realization by MATLAB. *2011 19th International Conference on Geoinformatics*, Jun, 1–4.

Gweba, B. 2018. *Developing a methodology for the assessment of wave energy along the South African Coast.* M.Phil. thesis, Stellenbosch University, Stellenbosch: South Africa.

Halliday, J. R., & Dorrell, D. G. 2004. Review of wave energy resource and wave generator developments in the UK and the rest of the world. *Pages 76–83 of: Proceedings of the 4th IASTED International Conference on Power and Energy Systems.*

Hasselmann, K. 1974. On the spectral dissipation of ocean waves due to white capping. *Boundary-Layer Meteorology*, **6**(1-2), 107–127.

Hasselmann, K., Barnett, T. P., Bouws, E., Carlson, H., Cartwright, D. E., Enke, K., Ewing, J. A., Gienapp, H., Hasselmann, D. E., Kruseman, P., Meerburg, A., Müller, P., Olbers, D.J., Richter, K., Sell, W., & Walden, H. 1973. Measurements of wind-wave growth and swell decay during the Joint North Sea Wave Project (JONSWAP). *Ergänzungsheft 8-12.*

Hayer, S., & Andersen, O. J. 2000. Freak waves: rare realizations of a typical population or typical realizations of a rare population? *In: The Tenth International Offshore and Polar Engineering Conference.* International Society of Offshore and Polar Engineers.

Komen, G. J., Hasselmann, S., & Hasselmann, K. 1984. On the existence of a fully developed wind-sea spectrum. *Journal of physical oceanography*, **14**(8), 1271–1285.

Lakhan, V. C. 2003. *Advances in coastal modeling.* Vol. 67. Elsevier.

Lavrenov, I. V. S. 1998. The wave energy concentration at the Agulhas current off South Africa. *Natural hazards*, **17**(2), 117–127.

Lawton, G. 2001. Monsters of the deep. *New Scientist*, **170**(2297), 28–32.

Longuet-Higgins, M. S. 1974. Breaking waves in deep or shallow water. *In: Proc. 10th Conf. on Naval Hydrodynamics*, vol. 597. MIT.

MacHutchon, K. R. 2006. *The Characterisation of South African Sea Storms.* Ph.D. thesis, Stellenbosch University, Stellenbosch: South Africa.

Mallory, J. K. 1974. Abnormal waves on the south-east coast of South Africa. *The International Hydrographic Review*, **51**(2), 99–129.

Miles, J. W. 1957. On the generation of surface waves by shear flows. *Journal of Fluid Mechanics*, **3**(2), 185–204.

Müller, P., Garrett, C., & Osborne, A. 2005. MEETING REPORT — Rogue Waves—The Fourteenth 'Aha Huliko'a Hawaiian Winter Workshop. *Oceanography*, **18**(3), 66–75.

Mori, N., Liu, P. C., & Yasuda, T. 2002. Analysis of freak wave measurements in the Sea of Japan. *Ocean Engineering*, **29**(11), 1399–1414.

Nikolkina, I., & Didenkulova, I. 2012. Catalogue of rogue waves reported in media in 2006–2010. *Natural Hazards*, **61**(3), 989–1006.

NOAA. 2019. *Catalog.* `https://data.nodc.noaa.gov/thredds/catalog/ncep/nww3/catalog.html`.

NSRI. 2019 (15 June). *Angler swept off rocks.* https://www.nsri.org.za/2019/06/angler-swept-off-rocks/.

NWS. 2017. *Environmental Modelling Center: NOAA NWS National Centers for Environmental Prediction.* `https://polar.ncep.noaa.gov/waves/hindcasts/`.

O'Brien, L, Dudley, J. M., & Dias, F. 2013. Extreme wave events in Ireland: 14 680 BP-2012. *Natural Hazards & Earth System Sciences*, **13**(3), 625–648.

Onorato, M., Osborne, A. R., Serio, M., & Bertone, S. 2001. Freak waves in random oceanic sea states. *Physical Review Letters*, **86**(25), 5831.

Osborne, A. R., Onorato, M., & Serio, M. 2000. The nonlinear dynamics of rogue waves and holes in deep-water gravity wave trains. *Physics Letters A*, **275**(5), 386–393.

Pelinovsky, E., & Kharif, C. 2003. Physical Mechanisms of the Rogue Wave Phenomenon. *European Journal of Mechanics - B/Fluids*, **22**(6), 603–634.

Peregrine, D. H. 1976. Interaction of water waves and currents. *Pages 9–117 of: Advances in applied mechanics*, vol. 16. Elsevier.

Pfaff, M. C., Logston, R. C., Raemaekers, S. J .P. N., Hermes, J. C., Blamey, L. K., Cawthra, H. C., Colenbrander, D. R., Crawford, R. J. M., Day, E., du Plessis, N., *et al.* 2019. A synthesis of three decades of socio-ecological change in False Bay, South Africa: setting the scene for multidisciplinary research and management. *Elem Sci Anth*, **7**(1).

Phillips, O. M. 1957. On the generation of waves by turbulent wind. *Journal of fluid mechanics*, **2**(5), 417–445.

Phillips, O. M. 1958. The equilibrium range in the spectrum of wind-generated waves. *Journal of Fluid Mechanics*, **4**(4), 426–434.

Pierson, W. J., & Moskowitz, L. 1964. A proposed spectral form for fully developed wind seas based on the similarity theory of SA Kitaigorodskii. *Journal of geophysical research*, **69**(24), 5181–5190.

Sand, S. E., Hansen, N. E. O., Klinting, P., Gudmestad, O. T., & Sterndorff, M. J. 1990. Freak wave kinematics. *Pages 535–549 of: Water wave kinematics.* Springer.

Shillington, F. A., & Schumann, E. H. 1993. High waves in the Agulhas Current. *Mariner's Weather Log Fall*, 24–28.

Shipley, A. M. 1964. Some Aspects of Wave Refraction in False Bay. *South African Journal of Science*, **60**(6), 115–120.

Smith, R. 1976. Giant waves. *Journal of Fluid Mechanics*, **77**(3), 417–431.

Theron, A., Rossouw, M., Rautenbach, C., von Saint Ange, U., Maherry, A., & August, M. 2013. *Determination of Inshore Wave Climate along the SA Coast - Phase 1 for Coastal Hazard and Vulnerability Assessment.* Tech. rept. Council of Scientific and Industrial Research, Stellenbosch.

Theron, A., Rossouw, M., Rautenbach, C., Page, P., Harribhai, J., Maherry, A., & von Saint Ange, U. 2014. *MetOcean Conditions and Vulnerability - Medium resolution wave climate and run-up.* Tech. rept. Council of Scientific and Industrial Research, Stellenbosch.

Touboul, J., Giovanangeli, J. P., Kharif, C., & Pelinovsky, E. 2006. Freak waves under the action of wind: experiments and simulations. *European Journal of Mechanics / B Fluids*, **25**(5), 662–676.

Veitch, J., Rautenbach, C. R., Hermes, J., & Reason, C. 2019. The Cape Point wave record, extreme events and the role of large-scale modes of climate variability. *Journal of Marine Systems*, 103185.

Violante-Carvalho, N., Parente, C. E., Robinson, I. S., & Nunes, L. M. P. 2002. On the growth of wind-generated waves in a swell-dominated region in the South Atlantic. *Journal of Offshore Mechanics and Arctic Engineering*, **124**(1), 14–21.

Williams, T. 2019. *On the importance of wind generated waves in embayments with complex orographic features – a South African case study.* Ph.D. thesis.

Willmott, C. J. 1982. Some comments on the evaluation of model performance. *Bulletin of the American Meteorological Society*, **63**(11), 1309–1313.

Woodroffe, C. D. 2002. *Coasts.* Cambridge [u.a.]: Cambridge Univ. Press.

Young, I. R. 1999. *Wind generated ocean waves.* Vol. 2. Elsevier.